Oxaliplatin Complexes with Carnosine and its Derivatives: *In Vitro* cytotoxicity, Mass Spectrometric and Computational Studies with a focus on Complex Fragmentation.

Eslam M. Moustafa[†], Claire L. Camp[⅄], Ahmed S. Youssef[‡], Asma Amleh[‡], Helen J. Reid[⅄], Barry L. Sharp[⅄] and Tamer Shoeib[†⅄*]

† Department of Chemistry, The American University in Cairo, New Cairo 11835, Egypt.

⅄ Centre for Analytical Science, Department of Chemistry, Loughborough University, Loughborough, Leicestershire LE11 3TU, UK.

‡ Department of Biology, The American University in Cairo, New Cairo 11835, Egypt.

[*] T.Shoeib@aucegypt.edu

Abstract

The complexation of the Pt-based anti-cancer drug oxaliplatin (OxPt) with biological ligands other than DNA is believed to be a major cellular sink for the drug reducing its therapeutic potential and acting as a potential cause of toxicity. In this paper, an *in vitro* study on hepatocellular carcinoma HepG2 cells suggests that the naturally abundant cytoplasmic dipeptide ligand *β*-alanyl-L-histidine dipeptide (carnosine) may inhibit the cytotoxic action of OxPt most likely through the formation of complexes that are less cytotoxic than OxPt alone. Evidence is provided to suggest that pre-exposure of HepG2 cells to elevated levels of carnosine appears to have a lasting effect on reducing the cytotoxicity of OxPt even after the removal of the carnosine. This effect, however, is shown to be under kinetic control as its magnitude was shown not to vary significantly with the level of carnosine exposure within the concentration range used in this study. Various mass spectrometry techniques employing electrospray ionization and chip nanospray were employed to study the interaction of oxaliplatin with carnosine as well as two of its derivatives being *β*-alanyl-*N*-methylhistidine (anserine) and *N*-Acetylcarnosine (NAC). Evidence of complexation between OxPt and each of the three ligands examined is presented. Most species observed were unambiguously assigned and compared to their theoretical isotopic patterns. Common fragmentation products due to the collisionally-activated protonated complexes of each of the ligands examined with OxPt, $[M + OxPt + H]^+$ where M= carnosine, anserine or NAC were reported. Density functional calculations at B3LYP/LANL2DZ were used to obtain structural information and relative free energies of different isomers of the observed precursor $[Carnosine + OxPt + H]^+$ both in the gas phase and in solution as well as to probe its fragmentation, highlighting plausible fragmentation mechanisms that account for all the experimental results.

Data are presented to show several binding modes between electron rich sites such as N and O centers of carnosine and the Pt metal of OxPt. Calculations were also employed to obtain proton affinities and free energies of key reactions. The proton affinities of carnosine, Anserine and NAC at 298 K were calculated to be 254.4, 255.9 and 250.2 kcal mol^{-1} respectively. To the best of our knowledge the proton affinities of anserine and N-acetyl-carnosine are the first reported values in the literature.

Introduction

Oxaliplatin (OxPt) is a third generation chemotherapeutic drug used in the treatment of colorectal cancer and cisplatin resistant cancers, [1-13] it was developed to overcome the nephrotoxicity of cisplatin and myelosuppression with carboplatin treatment. [14] Oxaliplatin has a broader range of activity than cisplatin and increased cytotoxicity over cis and carboplatin due to increased inhibition of DNA synthesis and greater efficiency in DNA repair. [13, 15, 16] The amine groups of cisplatin are replaced by diaminocyclohexane (dach) to form [Pt(dach)oxalate], oxaliplatin. The dach ligand is not recognised by mismatch repair complexes, which may explain its effectiveness in the treatment of cisplatin and carboplatin resistant cancers. [15]

The transport and interactions of oxaliplatin within cells is still not fully understood however,the simplistic route from blood to nuclear DNA involves the passive diffusion of oxaliplatin into the cell from the extracellular fluid where the Cl^- concentration is high (> 100 mM) into the cytoplasm, where the Cl^- concentration is low (4-20 mM). [17] The low Cl^- concentration in the cytoplasm results in the solvation of oxaliplatin, to its active forms $[Pt(OH_2)Cl(dach)]^+$ and $[Pt(OH_2)_2(dach)]^{2+}$[11,13], shown in Figure 1 and can interact with a plethora of non-DNA ligands. Based on previous work by Zayed *et. al.*[18] we can assume that the majority of the administered drug is found in the cell cytosol. It is thought that the

most likely sites for oxaliplatin interaction are the thiol groups of intercellular peptides and proteins. Recent studies have shown that the activated form of oxaliplatin forms very stable complexes with glutathione, being the most abundant low molecular weight thiol containing molecule in human cells. [19-21] However, work by this group [21, 22] and elsewhere [22, 23] suggests that Pt binding to intercellular peptides through their terminal amino nitrogen atoms and carbonyl oxygen atoms are possible and energetically competitive to sulphur attachment. This in combination with the large excess of these binding sites over those of sulphur raises the possibility of Pt adduction to non-thiol containing ligands in the proteome. All such non-DNA interactions are responsible for chemo-resistance and many of the side effects; including sensory-motor neuropathy, myelosuppression, gastrointestinal toxicity, idiosyncratic and hypersensitivity reactions. [24]

The endogenous dipeptide L-carnosine (*β*-alanyl-L-histidine) was discovered by Gulewitsch and Amiradzibi [25] from muscle tissue extracts in 1900 [26, 27] and is found in several organs including the brain (olfactory bulb and hippocampus) [28], cardiac muscle, kidney and stomach.[29, 30] In the skeletal muscle and nerve cells it is found at concentrations of up to 20 mM.[31, 32] Since its discovery there have been many investigations into its biological function and it is now known that carnosine acts as an anti-oxidant, scavenger of free radicals and active oxygen species [30], as a biological buffer, a source for histidine, an immuno-stimulant and transition metal ion chelator, especially for Zn^{2+} and Cu^{2+} [33] and heavy metals. [34] The ability of carnosine to bind Zn^{2+} helps modulate neuronal excitability by preventing the Zn^{2+} inhibition of neurotransmitter receptors. [35] Carnosine is also effective in the prevention and partial reversal of cataracts [36] and in the treatment of Wilsons disease [37] and Alzheimers due to its metal chelating and free radical scavenging ability and also acting as a β-amyloid toxicity inhibitor. [35, 38] It has also been shown that carnosine acts as a neuroprotector [39, 40] and can retard tumour growth in mouse models. [41] More recently

it has been reported that carnosine can prevent cell proliferation in colon cancer cells. [47, 48] The related dipeptides N-acetlycarnosine and anserine share many of the beneficial characteristics of carnosine. The N-acetyled form of carnosine, N-acetyl-carnosine has been shown to be effective in the treatment of stomach ulcers [42] and similarly to carnosine has been used in the treatment of cataracts. [43, 44] Anserine on the other hand, acts a chelator for copper and as an antioxidant as well as enhances the anti-tumour activity of doxorubicin. [45] Due to its presence in high abundance in the cytosolic fractions of cells [30] and its ability to scavenge transition metal elements we believe that the interactions between carnosine and oxaliplatin are of important scientific value. The investigation of the coordination chemistry of carnosine and oxaliplatin may provide new understanding in the mechanism of the cellular response to these drugs. Given that there are 1-5 Pt adducts per 10^6 nucleotides in patient white blood cells which represents approximately 10% of the total administered drug. [18] Assuming all nuclear Pt is bound to DNA, representing approximately 10^5 Pt atoms per cell, the majority of the administered drug is available to bind to other ligands such as proteins and peptides within the cell. With a large concentration of proteins per cell, approximately 10^6-10^7, [46] many with multiple binding sites, the potential for a wide range of Pt adducts to exist within the cell rather than specific Pt targets is a possible scenario. The interactions of carnosine and the related dipeptides anserine and N-acetylcarnosine with Oxaliplatin are therefore of great interest. By using a simple highly abundant dipeptide, such as carnosine to act as a simplified model of the broader Pt-meallome, we present detailed structural analysis of carnosine and the hydrolysed forms of oxaliplatin.

Instrumentation

An LTQ linear ion trap mass spectrometer with an electrospray source and a high resolution Q-Exactive Fourier transform mass spectrometer (Thermo Electron, San Jose, CA, USA)

were used. Both instruments were calibrated using Ultramark® 1621, caffeine and Met-Arg-Phe-Ala (MFRA) in accordance with the manufacturer's recommendations. The Q-Exactive was equipped with a Tri Versa NanoMate ESI chip nanospray (Advion, New York, USA). For the LTQ Resolving powers achieved were in the order of 1500 while the upper instrumental error limit in measurements was 0.2 m/z units. The LTQ auto-tune routine was used to obtain lens, quadrupole and octapole voltages for maximum transmission of the ions of interest. Helium gas, admitted into the ion trap at a maintained pressure of approximately 10^{-3}Torr, was used as the buffer gas to improve the trapping efficiency andas the collision gas for collision-induced dissociation (CID) experiments performed here at 15 eV in the lab frame. Experiments designed to elucidate ion structures or fragmentation pathways on the LTQ were performed as follows: the ion of interest was selected then collisionally activated by setting the activation amplitude at 25–35% of the maximum voltage available (determined empirically), and the activation Q setting (used to adjust the frequency of the RF excitation voltage) was set at 0.25 units. Sample solutions were continuously infused at a flow rate of 5 µl min^{-1} into the pneumatically assisted electrospray probe using dry nitrogen as the nebulising gas. Auxiliary and sheath gases were tuned daily for maximum signal transmission. Two tandem quadrupole mass spectrometers, An Acquity TQ and A XEVO TQ (Waters, MA, USA) both equipped with electrospray ionisation interface were also used in this work. Both triple quadrupoles were operated in positive ion mode, with typical values of cone, capillary and extractor voltages set to 30, 2500, and 3 respectively. The desolvation gas was usually set at a flow of 250 L h^{-1} and a temperature of 150 °C. Argon was used as the collision gas at a typical flow rate of 0.15 ml min^{-1}. Tandem mass spectra were obtained at collision energies in the range 5-25 eV in the lab frame having both Q1 and Q3 operated at unit resolution with typical a dwell time of 25 millisecond per transition.

Reagents

Carnosine, Anserine, HPLC-grade water and methanol were all purchased from Sigma-Aldrich, UK. N-Acetyl carnosine was purchased from Nanjing Gemsen international, China while oxaliplatin was obtained from Sanofi-Synthelabo Limited (Guildford, UK).

***In Vitro* cell viability assays**

To determine the *in vitro* effect of carnosine, the hepatocellular carcinoma cell line HepG2 was exposed to varying concentrations of OxPt, as well as several solution mixtures of OxPt and carnosine. The viability of HepG2 was assessed through MTT assay, which utilizes the conversion of the tetrazolium salt MTT (dimethylthiazol diphenyl tetrazolium bromide purchased from Serva, Germany) to formazan by dehydrogenase enzymes in living cells. [49] In brief, cells were cultured in 96-well plate (30,000 cells/well) at 37 ℃ humidified with 5% CO_2 in DMEM (Dulbecco's Modified Eagle Medium) supplemented with 10% FBS (Fetal bovine serum) and 5% Penicillin-Streptomycin mixture (Lonza, Switzerland). Cell counting was performed using Countess® Automated cell counter (Invitrogen). Solutions of OxPt at 8, 12, 16, 20, 24 and 28 μg ml^{-1}, as well as solution mixtures at varying molar ratios of carnosine at a fixed OxPt concentration of 24 μg ml^{-1} were made in the culture media. Each of the sample solutions made was incubated with the HepG2 cells for 24 hrs, wells containing cells treated only with media served as controls. After incubation the media was discarded, 20 μl MTT (5 mg/ml) and 100 μl fresh media were added to each well and incubated for 3 hours, all media was then discarded, and the purple formazan crystals formed were solubilized via the addition of 100 μl DMSO (Sigma-Aldrich, USA). The absorbance of each well was measured at 595 nm using a microplate reader FLUOstar OPTIMA (BMG LabTech,

Germany). Cell viability was determined by calculating the absorbance of the test wells as a percentage of the control wells.

Results and discussion

HepG2 cells showed decreased viability with exposure to increased concentrations of OxPt as shown in Figure 1. The most significant changes in cell viability were observed at exposure to OxPt concentrations of 16 μg ml^{-1} and greater as indicated by *P* values < 0.00001. To examine the *in vitro* effect of carnosine on OxPt cytotoxicity, several solutions were prepared at a fixed OxPt concentration of 24 μg ml^{-1} while varying the molar equivalent of carnosine. While the choice of OxPt concentration in these experiments was arbitrary, a value was chosen that corresponds to relatively low cell viability in order to easily observe the effects of subsequent addition of carnosine. It is also important to note that the OxPt concentration value chosen for these set of experiments was one that brought the most statistically significant decrease in the viability of the treated HepG2 cells as indicated by *P* values < 0.00001 (see Figure 1). The results of these experiments is shown in Figure 2 which points to a positive correlation between cell viability and increasing molar equivalence of canosine relative to OxPt. These differences were much less pronounced past the initial incremental addition of carnosine where a significant increase in cell viability was shown due to the exposure of a 1:1 molar ratio of carnosine to Oxpt relative to cells only exposed to OxPt at the same concentration and for the same incubation time. This was shown to be statistically significant with *P* value < 0.00001 at all non-zero molar ratios of carnosine to OxPt used. This result suggests that carnosine can interact with the OxPt drug forming complexes that reduce the drug's action.

In order to investigate the ability of carnosine to be passively diffused through cells, the same set of experiments were repeated but now cells were first incubated for 24 hours with

carnosine at various concentrations. After this incubation period, the media containing carnosine was discarded and fresh media containing 24 μg ml^{-1} of OxPt were added and allowed to incubate with the cells for a further 24 hour period. The results of these last set of *in vitro* experiment shown in Figure 3 indicate slight increased cell viability upon the exposure to carnosine. The much less pronounced effect shown in Figure 3 relative to that shown in Figure 2 is most likely due to the inability of carnosine to effectively passively diffuse through the cells. This also suggests that the process is kinetically controlled and is consistent with the near constant cell viability data obtained whenever the carnosine was present irrespective of the concentration at which it was allowed to incubate with the cells. While no claim is made that the *in vitro* data presented here replicates biological conditions in which OxPt and carnosine might interact, they do however indicate that the dipeptide carnosine has the ability to interact with OxPt most likely through the chelation of the platinum metal and thus if such interaction were present it may reduce the cytotoxic action of OxPt and thus warrants the investigation of such complexes.

To study the complexes of each of carnosine and its derivatives, anserine and N-acetyl-carnosine with oxaliplatin experiments were performed on four different mass spectrometers as detailed in the Instrumentation section. For the interest of conciseness, only selected representative results are shown here, however, all data are available in supplementary material. All sample solutions employed in this work were a 2 : 1 mM mixtures of either carnosine, anserine or N-acetyl-carnosine with oxaliplatin in a 1 : 1 (v/v) water/methanol solutions. Electrosparying each of these three solutions in the positive ion mode generated the mass spectra shown in Figures 4-6 (also see Figures S1 and S2 in supplementary material). In all cases, irrespective of the instrument used, the base peaks obtained were due to $[M + H]^+$ ions where M = carnosine, anserine or N-acetyl-carnosine. These ions corresponded to the signals at m/z values of 227, 241 and 269 shown in Figures 4, 5 and 6 (also see Figures

S1 and S2) respectively. Three other common ions were observed in each of the full scan MS spectra of the three solution mixtures examined here. Signals due to protonated oxaliplatin, $[OxPt + H]^+$, were always present as evidenced by the clusters observed in all full scan MS spectra obtained at around m/z 398. The lowest energy structure calculated for this protonated species was previously reported to have the external proton located on the 'inside' position of one of the oxalate carbonyl oxygen atoms. [21] Protonated ligand dimers, $[M_2 + H]^+$ ions, were also observed at m/z 453, 481 and 537 as seen in Figures 4, 5 and 6 (also see Figures S1 and S2). The third ion observed in all full scan MS spectra obtained was due to the $[M + OxPt + H]^+$ species as seen in the clusters around m/z 624, 637 and 666 in Figures 4 (also see Figure S1), 5 (also see Figure S2), and 6.

The assignments of these ions were confirmed by comparing the observed isotopic patterns to those theoretically modelled for each of the proposed species. For further confirmation the isotopic patterns for the proposed $[Carnosine + OxPt + H]^+$ and $[Anserine + OxPt + H]^+$ species being the focus of this study were obtained on the Q-Exactive FT-MS at a resolving power of about 60,000 and compared to their theoretical isotopic patterns at an equivalent resolution, the average error obtained over all the isotopic peaks observed were 2.13 and 1.48 ppm for $[Carnosine + OxPt + H]^+$ and $[Anserine + OxPt + H]^+$ respectively. This mass accuracy obtained without the use of lock masses provided unequivocal identifications as seen in Figures S3 and S4 of the supplementary material.

The significantly lower signal intensities of the $[OxPt + H]^+$ ion cluster centered at m/z 398 relative to the $[M + H]^+$ ions observed here as the base peaks in Figures 4-6 (also see Figures S1 and S2) was also observed previously where similar conditions were used but where M was glutathione. [21] Several explanations were given for this observations including the difference in proton affinities of OxPt and M. [21] The proton affinity of OxPt at 298 K was previously reported to be 233.5 kcal mol^{-1} [21] whereas the proton affinities for Carnosine,

anserine and N-acetyl-carnosine is calculated here to be 254.4, 255.9 and 250.2 kcal mol^{-1} respectively. To the best of our knowledge the proton affinities of anserine and N-acetyl-carnosine are the first reported values in the literature while three previously calculated values for the proton affinities of carnosine were given at 256.5 (at 0 K), [50] 245.4, [51] and 232.98, [52] kcal mol^{-1}. The latter of these values most likely needs to be revisited as it is significantly lower than all other calculated values and the only available experimental value for the proton affinity of carnosine of 244.59 kcal mol^{-1} obtained by the Graham Cooks method [51]. The proton affinities for Carnosine , anserine and N-acetyl-carnosine calculated here are in agreement with the lower $[OxPt + H]^+$ signal intensity relative to each of their respective protonated $[M + H]^+$ ions observed here.

Figures 7-9 and S5 of the supplementary material show the MS^2 spectra obtained by the mass selection followed by the subsequent fragmentation of each of the three $[M + OxPt + H]^+$ species, where M= carnosine, anserine and N-acetyl-carnosine. These spectra indicate common fragmentation pathways leading to the generation of several common ions being $[M + H]^+$, $[OxPt + H]^+$, $[M + OxPt - CO_2 + H]^+$, $[M - H + Pt(dach)]^+$ where M= carnosine, anserine and N-acetyl-carnosine; OxPt is oxaliplatin and dach is diaminocyclohexane as indicated earlier in the text.

The precursor ion $[Carnosine + OxPt + H]^+$ were theoretically examined in great detail in the gas phase and in solution as this complex is most likely formed initially in the solution mixture used here. The potential energy surfaces of this complex in the gas phase and in solution were found to be relatively flat with several low lying minima as listed in Table 1 and shown in Figures 10 and 11. The calculated structures on these potential energy surfaces can be divided in two categories involving either direct Pt bonding to carnosine or electrostatic interactions between protonated carnosine and OxPt. The bonding category involves the substitution of a single Pt-oxygen bond of the oxalate moiety of OxPt by a

formal Pt-coordination to an electron rich site on the carnosine substrate; this typically being one of the imidazole nitrogen atoms, a carbonyl oxygen or the terminal amino nitrogen of the dipeptide as shown in Figure 11. The electrostatic category on the other hand involves electrostatic interactions between the oxaliplatin molecule and protonated carnosine through hydrogen bonding which are responsible for keeping the resulting [Carnosine + OxPt + H]$^+$ complex together as shown in Figure 11. It is interesting to note that all the structures constituting this category involve the formal protonation of the carnosine ligand as opposed to OxPt. This is consistent with the higher calculated proton affinity of carnosine relative to Oxpt as discussed earlier. Structures in the first and latter of these categories calculated to be within about 15 kcal mol^{-1} in free energy of both the gas phase and solution global minina found are shown in Figures 10 and 11 respectively, while all structures calculated on this potential energy surface are listed in Table S1 in supplementary material. Seven of the eleven structures shown in Figure involve Pt coordination to either the *pros* or *tele* nitrogen atoms of the histidine ring of carnosine. Structures **1A**, **1B** and **1D** in Figure 10, all resulting in the cluster centred on m/z 624 as seen in Figure 4 and Figures S1 and S3 of the supplementary material, comprise the two lowest energy conformers in the gas phase and the lowest two energy conformers in solution on these potential energy surfaces. These three structures all involve Pt coordination to the *pros* nitrogen atoms of the histidine ring of carnosine and formal protonation on one of the carbonyl oxygen atoms of the oxalate moiety of oxaliplatin. This is consistent with an earlier study examining the silver ion binding energies of all 20 α-amino acids, showing that histidine had the third highest silver ion binding energy being lower than that of arginine and only slightly lower than that of lysine. [53] The lowest energy conformer of the Ag^+-histidine complex in that perious study also showed Pt-coordination to the *pros* nitrogen atoms of the histidine ring. [53] Here, the global minimum on the gas phase potential energy surface is structure **1A** as shown in Figure 10, this structure is internally

stabilised by four strong hydrogen bonds making it 3.4 kcal mol^{-1} lower in energy in the gas phase relative to **1D** and only 0.8 kcal mol^{-1} removed from the lowest energy structure calculated on the solution phase potential energy surface being structure **1D** as shown in Figure 10. Structure **1D** is also stabilised by two internal hydrogen bonds. It is interesting to note that in the gas phase structure **1A** the hydrogen bond between one of the NH hydrogen atoms of the dach ligand and the carboxylic oxygen of the terminal carboxylate group being at 1.886 Å becomes none existent in solution (distance of 5.297 Å as shown in Figure 10) as it is replaced by external solvation. The strongest hydrogen bonds in either the two gas phase structures, **1A** and **1D**, is between each of the hydrogen atoms of the protonated oxalate moieties and their respective terminal amino nitrogen atom of each of the carnosine dipeptides. This is determined based on the shortest hydrogen bonding distance calculated in either gas phase structure being 1.315 and 1.328 Å for structures **1A** and **1D** respectively as well as on the resulting hydrogen bonding angles being closest to the ideal linear arrangement calculated to be 166° for the N-H-O in both cases.

In the solution phase on the other hand structures **1A** and **1D** both have their terminal amino nitrogen atoms protonated while forming strong hydrogen bonds to a carboxylic oxygen atom of the oxalate moiety in each case at 1.509 and 1.496 Å respectively. If the solution phase structures **1A** or **1D** being the two lowest energy structures on that potential energy surface are transferred to the gas phase by solvent evaporation through the soft electrospray ionisation technique while maintaining the protonation on the terminal amino nitrogen atom a structure **1K** or **1I** would result, this structure is similar to **1C** with the noted difference that structure **1C** involves Pt coordination to the *tele* nitrogen of the histidine ring. Structure **1K** is calculated to be energetically competitive in the gas phase and in solution being only 8.7 and 2.7 kcal mol^{-1} removed from either global minina respectively. Alternatively, the gas-phase transfer of the hydrogen atom of the protonated oxalate moiety to the terminal amino

nitrogen atom in either gas phase structure **1A** or **1D** while maintaining the Pt coordination to the *pros* nitrogen of histidine would also results in the formation of structure **1K** or **1I**. The loss of CO_2 from the deprotonated oxalate moiety of this resulting structure, **1K** or **1I**, followed by a proton transfer from the formally protonated NH_3^+ group of the carnosine dipeptide to the carbon atom of the remaining CO_2 group of the oxalate moiety of results in the formation of structure **2A** shown in Figure 12. Structure **2A** is the lowest energy structure calculated for the $[Carnosine + OxPt - CO_2 + H]^+$ species observed as the m/z cluster around 580 in the MS^2 spectra shown in Figure 4 and as the signals at m/z 579, 580 and 581 for ^{194}Pt, ^{195}Pt and ^{196}Pt as shown in panels A, B and C of Figure S5 respectively. Structure **2A** is shown to contain three internal hydrogen bonds which help stabilise it. It is interesting to note that the lowest three energy structures calculated for the $[Carnosine + OxPt - CO_2 + H]^+$ species, assigned as the cluster centred on m/z 580 as seen in Figure 7 and resulting in the signals at m/z 579, 580 and 581 in panels A, B and C respectively of Figure S5 of the supplementary material also all involve Pt-coordination to the *Pros* nitrogen atom of the hystidine ring of the carnosine dipeptide. Structures **2B** and **2C** are calculated to be only 2.6 and 5.9 kcal mol^{-1} higher in free energy relative to structure **2A** respectively. The gas phase inter-conversion between these three structures is expected to be rapid and well within the energies available under the collision induced dissociation conditions employed here as they involve simple rotations about single bonds. Interestingly, structure **2C** involves a hydrogen bond at 1.765 Å between the OH hydrogen of the carboxylate group of the carnosine dipeptide and the Pt-bound oxygen atom of the remaining HCO_2 group of the oxalate moiety. The transfer of this hydrogen atom from the OH group to the carboxylate group of carnosine followed by the neutral loss of the resulting H_2CO_2 group and the subsequent binding of the resulting carboxylic oxygen to the Pt center results in structure **3A** shown in Figure 13. Structure **3A** is calculated to be the lowest structure for the $[Carnosine - H + Pt(dach)]^+$

species assigned as the cluster centered on mz/534 in Figure 7 and the signals at m/z 533, 534 and 535 in panels A, B and D respectively in Figure S5 of the supplementary material. This assignment was further confirmed by the isotopic pattern obtained on the high resolution Q-Exactive FT-MS shown in Figure S6 of the supplementary material. The formation of the [Carnosine – H + Pt(dach)]$^+$ species from the [Carnosine + OxPt – CO_2 + H]$^+$ precursor is supported by the MS^3 spectrum in Figure S7 clearly showing the cluster centred on m/z 534 being the dominant fragment due to the dissociation the[Carnosine + OxPt – CO_2 + H]$^+$ precursor.

The two other signals observed at significantly lower intensities in Figure S7 are the clusters centred on m/z 517 and 354. These signals were also weak signals observed in the MS^2 spectrum of [Carnosine + OxPt + H]$^+$ shown in Figures 7 and S5 of the supplementary material and were assigned as [Carnosine – NH_3 – H + Pt(dach)]$^+$ and [OxPt – CO_2 + H]$^+$ respectively. The latter of these species is most likely produced via the neutral loss of carnosine from [Carnosine + OxPt – CO_2 + H]$^+$ species clustered on m/z 580 generating the ion [OxPt – CO_2 + H]$^+$, Structures **5A** and **5B** in Table 1. The lowest energy of these two structures contains a Pt centre that is dicoordinated to the dach ligand while forming two other symmetrical bonds to either oxygen atom of the COOH moiety.

The species observed as a cluster centred on m/z 517 assigned as [Carnosine – NH_3 – H + Pt(dach)]$^+$ is most likely due to the loss of NH_3 from [Carnosine – H + Pt(dach)]$^+$ as confirmed by MS^4 data (not shown). Here, a 1,3 hydride shift to the terminal amino nitrogen atom of the lowest energy species on the [Carnosine – H + Pt(dach)]$^+$ surface, Structure **3A**, and the subsequent loss of the resulting NH_3 group results in the formation of the lowest energy structure calculated for the [Carnosine – NH_3 – H + Pt(dach)]$^+$ species, structure **4A**, being the lowest energy species on this surface as shown in Figure 14.

Conclusions

In this paper, *in vitro* studies on hepatocellular carcinoma HepG2 cells suggest that the dipeptide carnosine may inhibit the cytotoxic action of OxPt most likely through the formation of complexes that are less cytotoxic than OxPt alone. Evidence was provided to suggest that pre-exposure of HepG2 cells to elevated levels of carnosine appears to have a lasting effect on reducing the cytotoxicity of OxPt even after the removal of the carnosine. This effect, however, was shown to be under kinetic control as its magnitude was shown not to vary significantly with the level of carnosine exposure within the concentration range used in this study. Various mass spectrometry techniques employing electrospray ionization and chip nanospray were employed to study the interaction of oxaliplatin with the naturally abundant cytoplasmic dipeptide ligand *β*-alanyl-L-histidine (carnosine) as well as two of its derivatives being *β*-alanyl-*N*-methylhistidine (anserine) and *N*-Acetylcarnosine (NAC). Evidence of complexation between OxPt and each of the three ligands examined is presented. Most species observed were unambiguously assigned and compared to their theoretical isotopic patterns. Common fragmentation products due to the collisionally-activated protonated complexes of each of the ligands examined with OxPt, $[M + OxPt + H]^+$ where M= carnosine, anserine or NAC were shown to be $[OxPt - CO_2 + H]^+$, $[OxPt + H]^+$, $[M - H + Pt(dach)]^+$, $[M + OxPt - CO_2 + H]^+$ and $[M + H]^+$. Density functional calculations at B3LYP/LANL2DZ were used to obtain structural information and relative free energies of different isomers of the observed precursor $[Carnosine + OxPt + H]^+$ and the fragments produced highlighting plausible fragmentation mechanisms that account for all the experimental results. Data presented showed several binding modes between electron rich sites such as N and O centers of Carnosine and the Pt metal of OxPt. Values for proton affinities of carnosine, anserine and NAC at 298 K were calculated to be 254.4, 255.9 and 250.2 kcal mol^{-1} respectively.

Acknowledgements

The authors would like to thank the EPSRC, NSCCS, LGC ltd., the Centre for Analytical Science at Loughborough University, the American University in Cairo and the Centre for Innovative and Collaborative Engineering at Loughborough University for the funding sponsorship and provision of resources for the project. Samir Nabhan of the Department of Chemistry as well as Aya Youssef and Mariam Rizkallah of the Department of Biology both at the American Univerity in Cairo are acknowledged for technical assistance. We are grateful for Dr. Mehmet Ozturk from the Department of Molecular Biology and Genetics, Bilkent University for providing us with the HepGe cell line.

References

1. Y. Yue, X. Chen, J. Qin and X. Yao, *ColloidSurface B*, 2009, **69**, 51-57.
2. O. Rixe, W. Ortuzar, M. Alvarez, R. Parker, E. Reed, K. Paull and T. Fojo, *Biochem. Pharmacol.*, 1996, **52**, 1855-1865.
3. A. Carrato, J. Gallego and E. Díaz-Rubio, *Crit. Rev. Oncol.*, 2002, **44**, 29-44.
4. A. de Gramont, A. Figer, M. Seymour, M. Homerin, A. Hmissi, J. Cassidy, C. Boni, H. Cortes-Funes, A. Cervantes, G. Freyer, D. Papamichael, N. Le Bail, C. Louvet, D. Hendler, F. de Braud, C. Wilson, F. Morvan and A. Bonetti, *J. Clin. Oncol.*, 2000, **18**, 2938-2947.
5. A. Riccardi, C. Ferlini, D. Meco, R. Mastrangelo, G. Scambia and R. Riccardi, *Eur. J. Cancer*, 1999, **35**, 86-90.
6. E. Raymond, C. Buquet-Fagot, S. Djelloul, J. Mester, E. Cvitkovic, P. Allain, C. Louvet and C. Gespach, *Colloq. Inse*, 1997, **8**, 876-885.
7. R. Mandal, R. Kalke and X. Li, *Chem. Res. Toxicol.*, 2004, **17**, 1391-1397.
8. T. Connors, M. Jones, W. Ross, P. Braddock, A. Khokhar and M. Tobe, *Chem. Biol. Interact.*, 1972, **5**, 415-424.
9. S. Chaney, S. Campbell, B. Temple, E. Bassett, Y. Wu and M. Faldu, *J. Inorg. Biochem.*, 2004, **98**, 1551-1559.
10. D. Machover, E. DiazRubio, A. deGramont, A. Schilf, J. J. Gastiaburu, S. Brienza, M. Itzhaki, G. Metzger, D. NDaw, J. Vignoud, A. Abad, E. Francois, E. Gamelin, M. Marty, J. Sastre, J. F. Seitz and M. Ychou, *Ann. Oncol.*, 1996, **7**.
11. S. Chaney and A. Vaisman, *J. Inorg. Biochem.*, 1999, **77**, 71-81.
12. J. M. Woynarowski, S. Faivre, M. C. S. Herzig, B. Arnett, W. G. Chapman, A. V. Trevino, E. Raymond, S. G. Chaney, A. Vaisman, M. Varchenko and P. E. Juniewicz, *Mol. Pharmacol.*, 2000, **58**, 920-927.

13. E. Raymond, S. Chaney, A. Taamma and E. Cvitkovic, *Ann. Oncol.*, 1998, **9**, 1053-1071.
14. H. Ito, H. Yamaguchi, A. Fujikawa, N. Tanaka, A. Furugen, K. Miyamori, N. Takahashi, J. Ogura, M. Kobayashi, T. Yamada, N. Mano and K. Iseki, *J. Pharm. Biomed. Anal.*, 2012, **71**, 99-103.
15. A. Carrato, J. Gallego and E. Diaz-Rubio, *Crit. Rev. Oncol. Hemat.*, 2002, 44, 29-44.
16. I. Gourdier, M. Del Rio, L. Crabbé, L. Candeil, V. Copois, M. Ychou, C. Auffray, P. Martineau, N. Mechti, Y. Pommier and B. Pau, *FEBS Lett.*, 2002, **529**, 232-236.
17. F. Arnesano and G. Natile, *Coord. Chem. Rev.*, 2009, **253**, 2070-2081.
18. A. Zayed, T. Shoeib, S. E. Taylor, G. D. D. Jones, A. L. Thomas, J. P. Wood, H. J. Reid and B. L. Sharp, *Int. J. Mass Spectrom.*, 2011, **307**, 70-78.
19. R. Jelic, S. Markovic and B. Petrovic, *Monatshefte Fur Chemie*, 2011, **142**, 985-992.
20. K. Wang, J. Lu and R. Li, *Coord. Chem. Rev.*, 1996, **151**, 53-88.
21. T. Shoeib and B. L. Sharp, *Metallomics*, 2012, **4**, 1308-1320.
22. D. V. Deubel, *J. Am. Chem. Soc.*, 2004, **126**, 5999-6004.
23. D. V. Deubel, *J. Am. Chem. Soc.*, 2002, 124, 5834-5842.
24. C. G. Hartinger, Y. O. Tsybin, J. Fuchser and P. J. Dyson, *Inorg. Chem.*, 2008, **47**, 17-19.
25. W. Gulewitsch and S. Amiradzibi, *Ber Deut Chem Ges*, 1900, **33**, 1902-1903.
26. I. Severina, O. Bussygina and N. Pyatakova, *Biochemistry-Moscow*, 2000, **65**, 783-788.
27. R. Kohen, Y. Yamamoto, K. Cundy and B. Ames, *Proc. Natl. Acad. Sci. U. S. A.*, 1988, 85, 3175-3179.
28. M. Horning, L. Blakemore and P. Trombley, *Brain Res.*, 2000, **852**, 56-61.
29. O. Aruoma, M. Laughton and B. Halliwell, *Biochem. J.*, 1989, **264**, 863-869.
30. S. E. Gariballa and A. J. Sinclair, *Age Ageing*, 2000, **29**, 207-210.

31. G. Begum, A. Cunliffe and M. Leveritt, *Int. J. Sport Nutr. Exerc. Metab.*, 2005, **15**, 493-514.
32. F. Bellia, G. Vecchio, S. Cuzzocrea, V. Calabrese and E. Rizzarelli, *Mol. Aspects Med.*, 2011, **32**, 258-266.
33. A. R. Hipkiss and C. Brownson, *Biogerontology*, 2000, **1**, 217-223.
34. P. J. Quinn, A. A. Boldyrev and V. E. Formazuyk, *Mol. Aspects Med.*, 1992, **13**, 379-444.
35. C. Corona, V. Frazzini, E. Silvestri, R. Lattanzio, R. La Sorda, M. Piantelli, L. M. T. Canzoniero, D. Ciavardelli, E. Rizzarelli and S. L. Sensi, *PLoS ONE*, 2011, **6**, e17971.
36. M. Babizhayev, *Biochim. Biophys. Acta*, 1989, **1004**, 363-371.
37. J. Kang, K. Kim, S. Choi, H. Kwon, M. Won and T. Kang, *Mol. Cells*, 2002, **13**, 498-502.
38. J. E. Preston, A. R. Hipkiss, D. T. J. Himsworth, I. A. Romero and J. N. Abbott, *Neurosci. Lett.*, 1998, **242**, 105-108.
39. S. Stvolinsky, M. Kukley, D. Dobrota, M. Vachova, I. Tkac and A. Boldyrev, *Cell. Mol. Neurobiol.*, 1999, **19**, 45-56.
40. A. Boldyrev, S. Stvolinsky, O. Tyulina, V. Koshelev, N. Hori and D. Carpenter, *Cell. Mol. Neurobiol.*, 1997, **17**, 259-271.
41. C. Renner, N. Zemitzsch, B. Fuchs, K. D. Geiger, M. Hermes, J. Hengstler, R. Gebhardt, J. Meixensberger and F. Gaunitz, *Mol. Cancer*, 2010, **9**, 2.
42. M. Seiki, S. Ueki, Y. Tanaka, M. Soeda, Y. Hori, H. Aita, T. Yoneta, H. Morita, E. Tagashira and S. Okabe, *Folia Pharmacol. Jap.*, 1990, **95**, 257-269.
43. M. A. Babizhayev, *Fundam. Clin. Pharmacol.*, 2012, **26**, 86-117.
44. M. Babizhayev, A. Deyev, V. Yermakova, Y. Semiletov, N. Davydova, N. Kurysheva, A. Zhukotskii and I. Goldman, *Peptides*, 2001, **22**, 979-994.

45. Y. Sadzuka and T. Sonobe, *Food Chem. Toxicol.*, 2007, **45**, 985-989.
46. C. Vogel, S. A. de, D. Ko, S. Le, B. A. Shapiro, S. C. Burns, D. Sandhu, D. R. Boutz, E. M. Marcotte and L. O. Penalva, *Mol Syst Biol*, 2010, 6.
47. B. Iovine, M. L. Iannella, F. Nocella, M. R. Pricolo and M. A. Bevilacqua, *Cancer Lett.*, 2012, 315, 122-128.
48. Y. Horii, J. Shen, Y. Fujisaki, K. Yoshida and K. Nagai, *Neurosci. Lett.*, 2012, 510, 1-5.
49. Wilson, J. K., Sargent, J. M., Elgie, A. W., Hill, J. G., & Taylor, C. G. (1990) *British Journal of Cancer 62*(2), 189–194
50. Menges, F.; Riehn, C.; Niedner-Schatteburg, G. The Interaction of the Dipeptide Carnosine With Alkali Metal Ions Studied by Ion Trap Mass Spectrometry. *Z. Phys. Chem.* **2011**, *225*, 595-609.
51. Cheng, M. K. Mass spectrometric and theoretical studies on protonated and potassium cationized biological molecules in the gas phase, Hong Kong Polytechnic University (Hong Kong), Hong Kong, 2007.
52. Björn M. Reinhard. Chemistry of microsolvated metal ions, TU Kaiserslautern, Germany, 2003.
53. J. Phys. Chem A, 106, 25, 2002

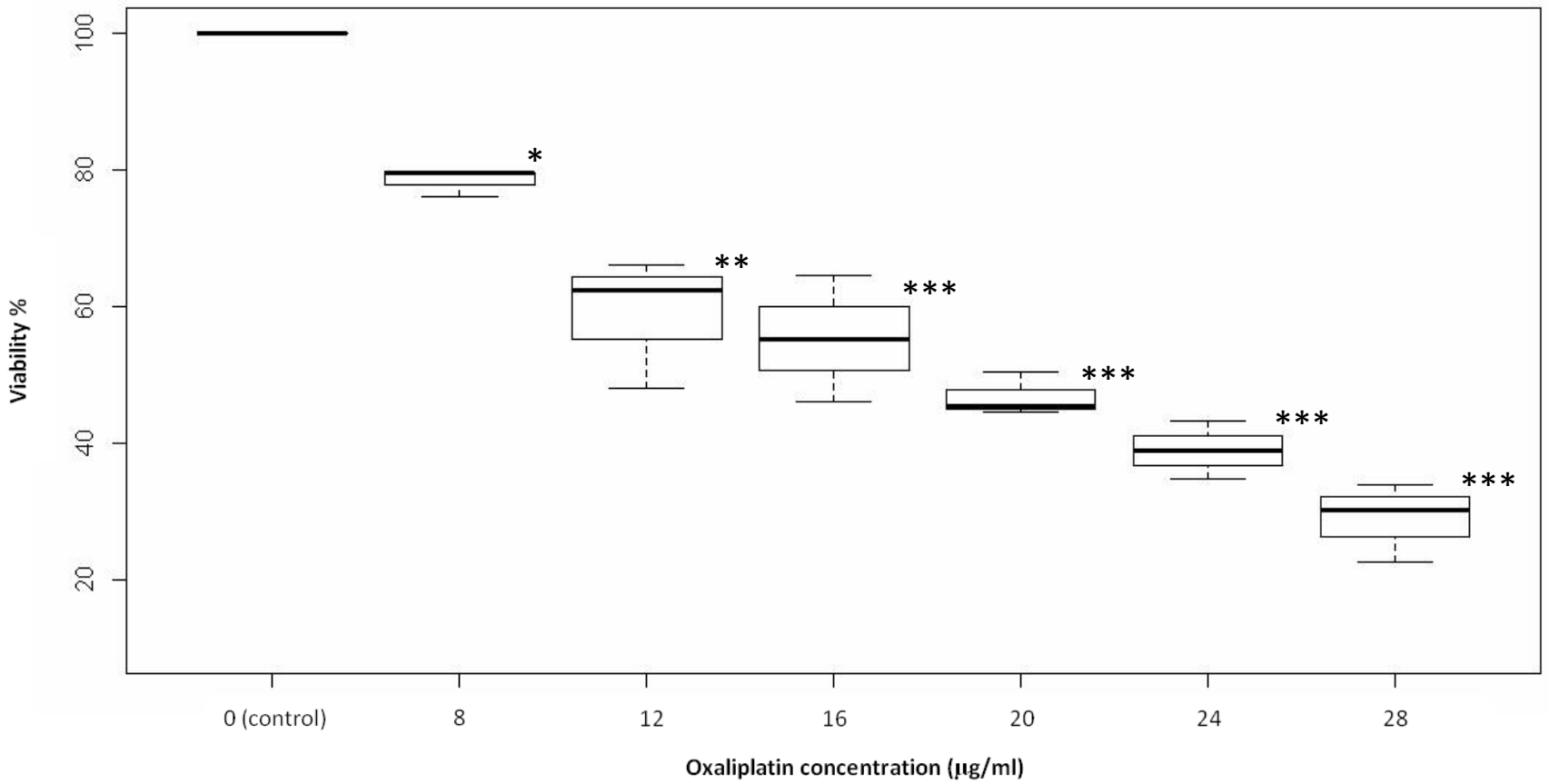

Figure 1. Percent viability of HepG2 cells upon exposure to varying concentrations of Oxaliplatin for 24 hours. Each data point within an experiment is the average of three separate runs. The data presented here in boxplot format are the average of three separate experiments. Error bars represent the Standard error of deviation and the statistical significance is represented by * for P <0.01, ** for P <0.0001 and *** for P < 0.00001

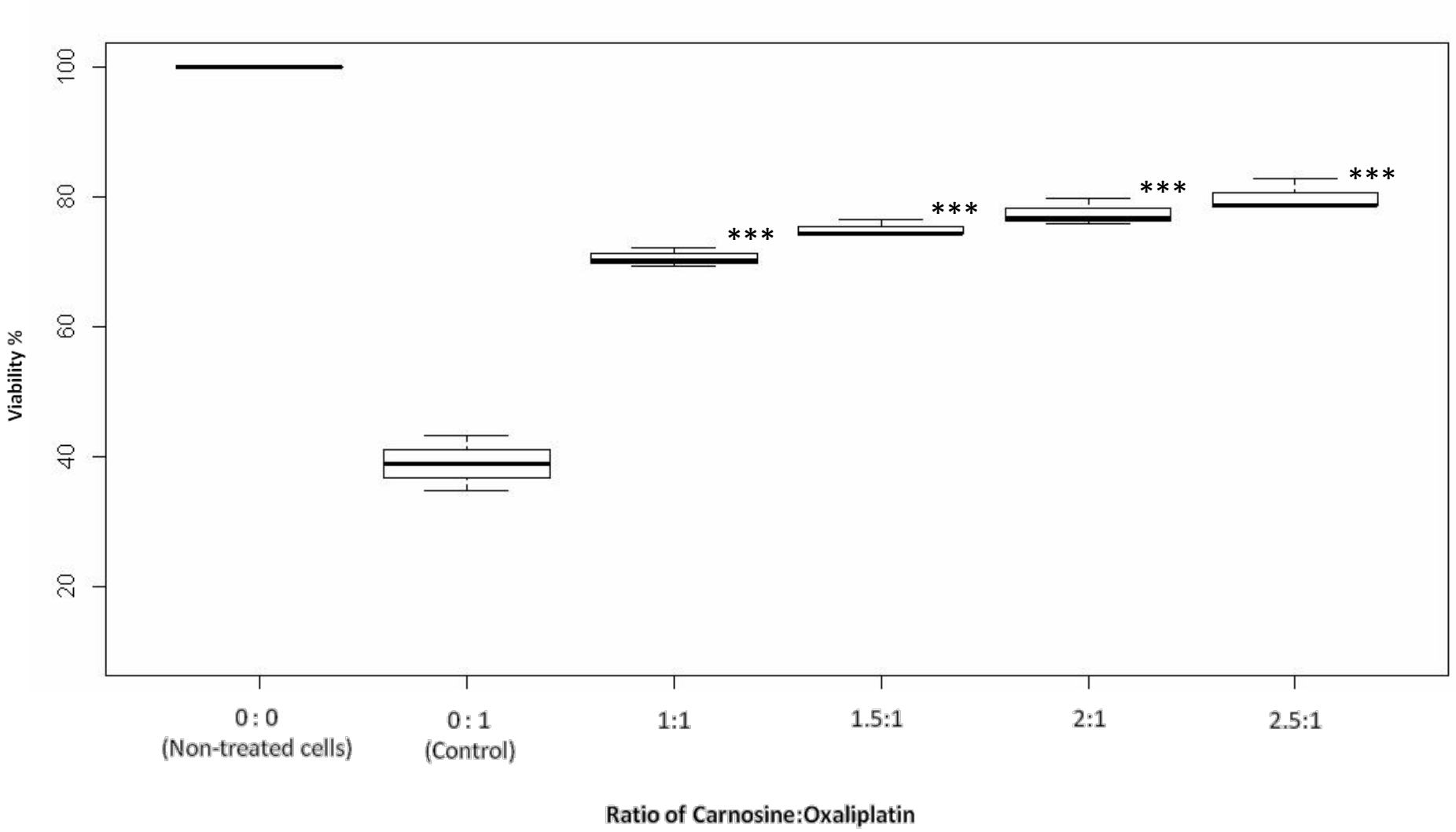

Figure 2. Percent viability of HepG2 cells upon exposure to increasing molar ratios of carnosine in the presence of 24μg ml^{-1} oxaliplatin for 24 hours. Values at (0:1, 1:1, 1.5:1, 2:1 and 2.5:1) refer to the molar ratios of carnosine to oxaliplatin. Each data point within an experiment is the average of three separate runs. The data presented here in boxplot format are the average of three separate experiments. Error bars represent the Standard error of deviation and the statistical significance of the solution mixtures relative to 24 ug/ml Oxaliplatin is represented by * for $P<0.001$, ** for $P<0.0001$ and *** for $P<0.00001$

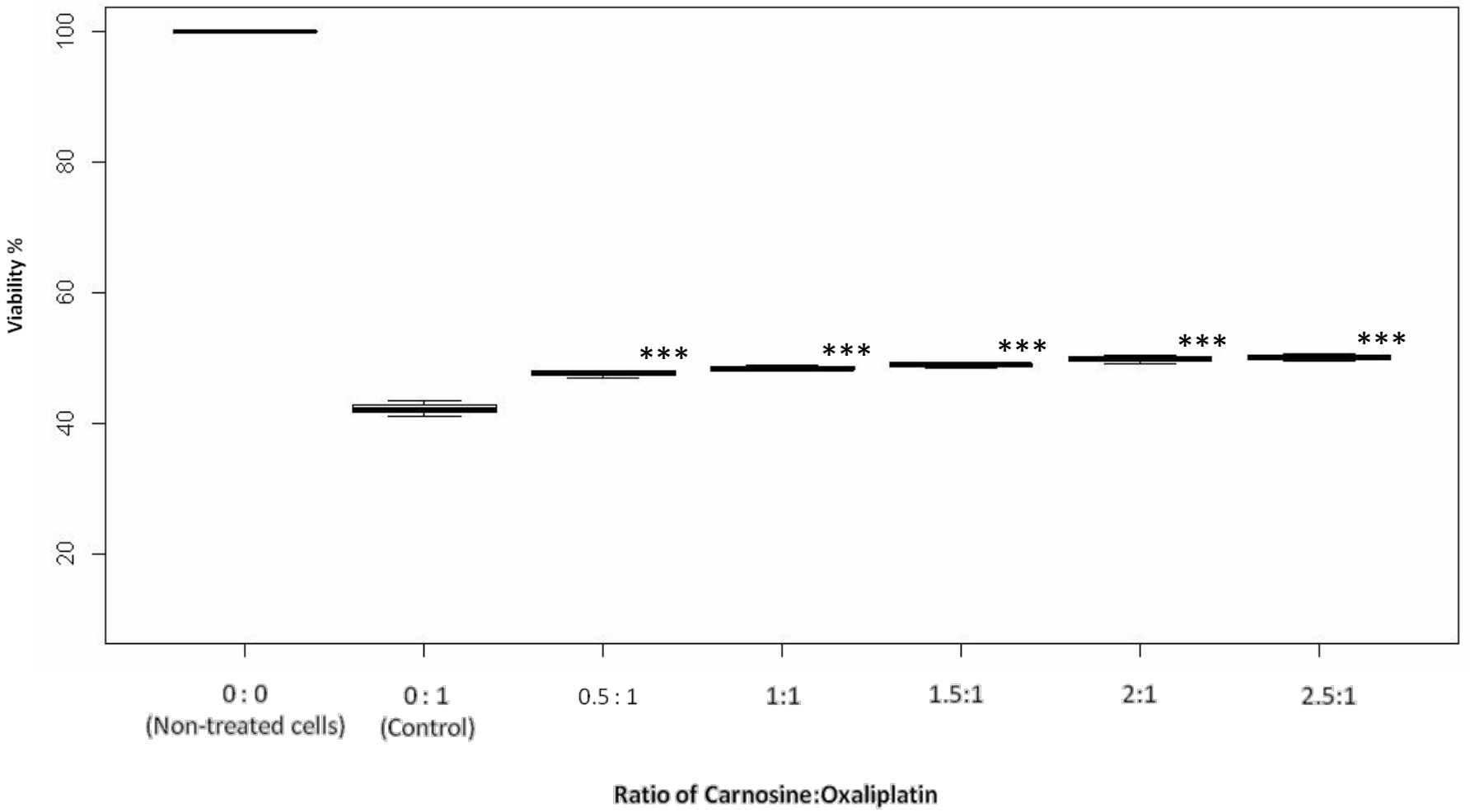

Figure 3. Percent viability of HepG2 cells upon the initial exposure to increasing carnosine concentrations followed by the exposure to 24μg ml^{-1} oxaliplatin for 24 hours. Values at (0.5:1, 1:1, 1.5:1, 2:1 and 2.5:1) refer to the molar ratios of carnosine to oxaliplatin. Each data point within an experiment is the average of three separate runs. The data presented here in boxplot format are the average of three separate experiments. Error bars represent the Standard error of deviation.

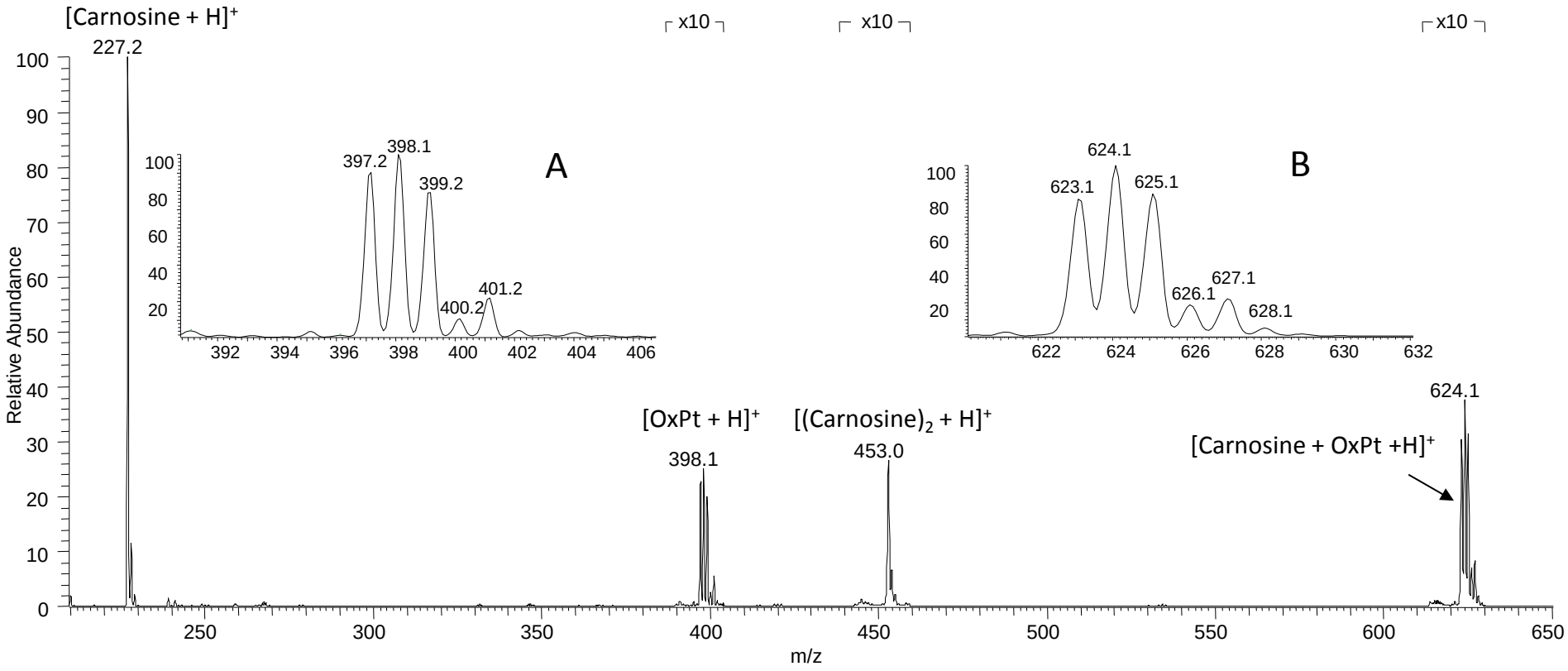

Figure 4: Full scan MS spectrum of a (2:1) molar mixture of Carnosine and OxPt in a (1:1) (v/v) water/methanol solution as obtained on the LTQ without allowing for incubation time. The sections of the spectrum shown under "x10" signify the magnification of the signal by 10 fold for clarity. This magnification means that for example the intensity of the ion at m/z 453.0 is about 3% of the base peak. The signals assigned as $[OxPt + H]^+$ and $[Carnosine + OxPt + H]^+$ are each expanded and normalized to 100% in inserts A and B respectively for clarity.

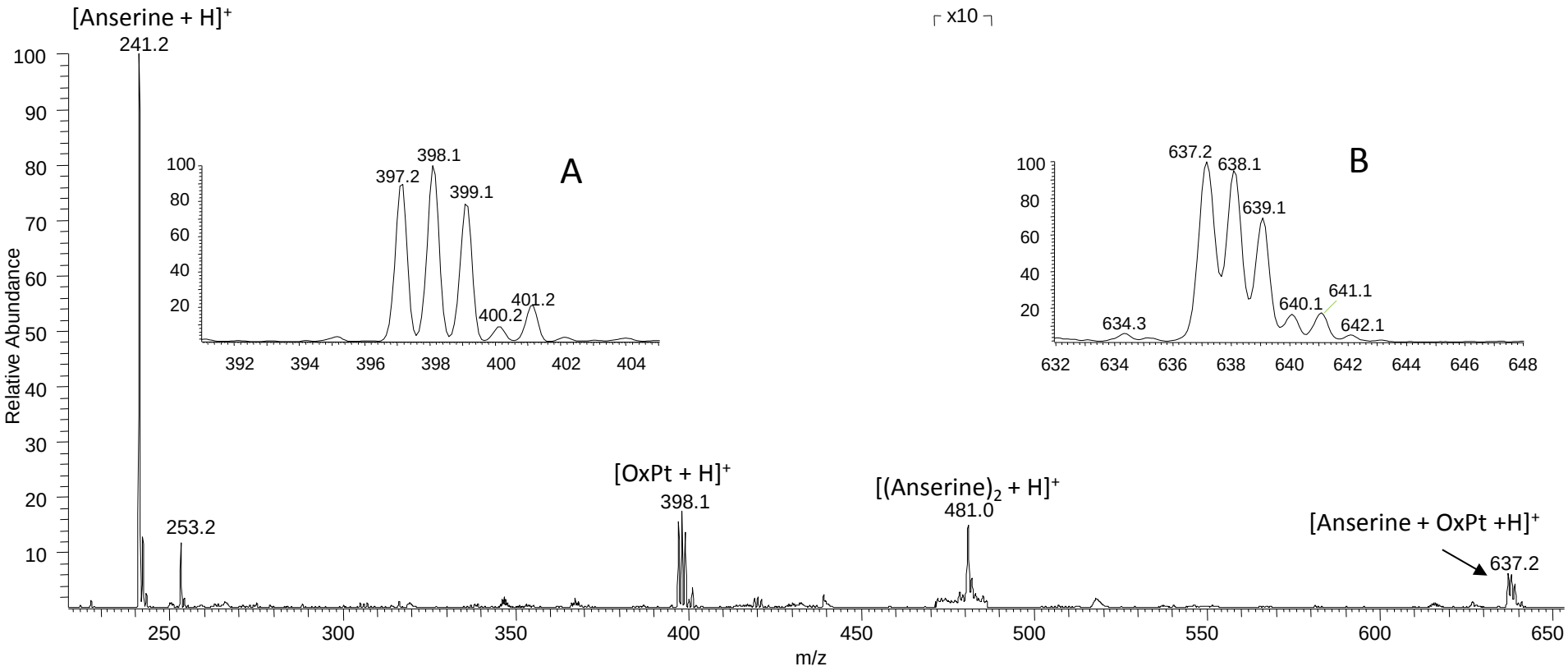

Figure 5: Full scan MS spectrum of a (2:1) molar mixture of Anserine and OxPt in a (1:1) (v/v) water/methanol solution as obtained on the LTQ without allowing for incubation time. The sections of the spectrum shown under "x10" signify the magnification of the signal by 10 fold for clarity. This magnification means that for example the intensity of the ion at m/z 481.0 is about 2% of the base peak. The signals assigned as $[OxPt + H]^+$ and $[Anserine + OxPt + H]^+$ are each expanded and normalized to 100% in inserts A and B respectively for clarity.

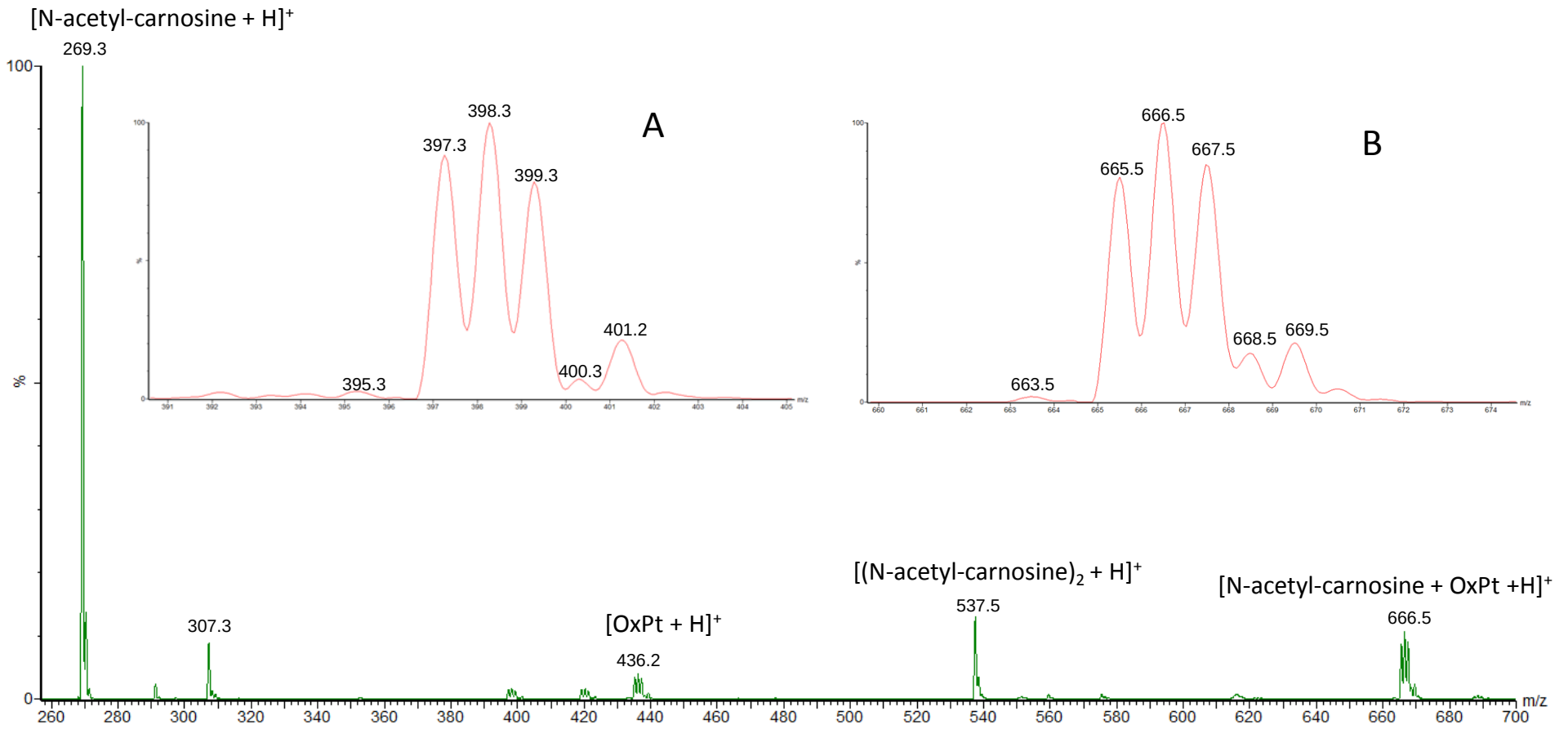

Figure 6: Full scan MS spectrum of a (2:1) molar mixture of N-acetyl-carnosine and OxPt in a (1:1) (v/v) water/methanol solution as obtained on the Acquity TQ without allowing for incubation time. The signals assigned as $[OxPt + H]^+$ and $[N\text{-acetyl-carnosine} + OxPt + H]^+$ are each expanded and normalized to 100% in inserts A and B respectively for clarity.

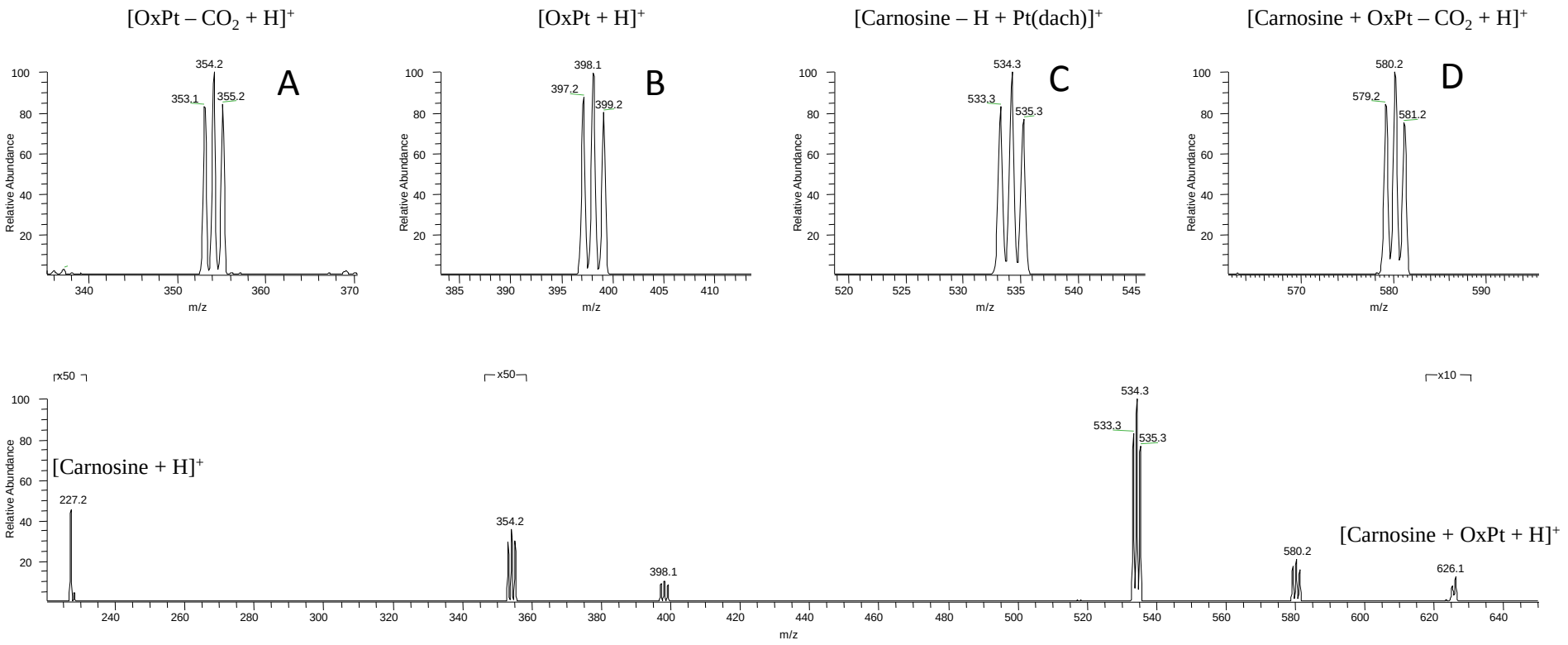

Figure 7: MS^2 spectrum of the entire isotopic envelope of the ion $[Carnosine + OxPt + H]^+$ generated at 15 ev in the lab frame and isolated from the full scan spectrum of a (2:1) molar mixture of Carnosine and OxPt in a (1:1) (v/v) water/methanol solution as obtained on the LTQ without allowing for incubation time. The sections of the spectrum shown under "x10" and "x50" signify the magnification of the signal by 10 and 50 fold respectively for clarity. The signals assigned as $[OxPt – CO_2 + H]^+$, $[OxPt + H]^+$, $[Carnosine – H + Pt(dach)]^+$ and $[Carnosine + OxPt – CO_2 + H]^+$ are each expanded and normalized to 100% in inserts A through D respectively for clarity.

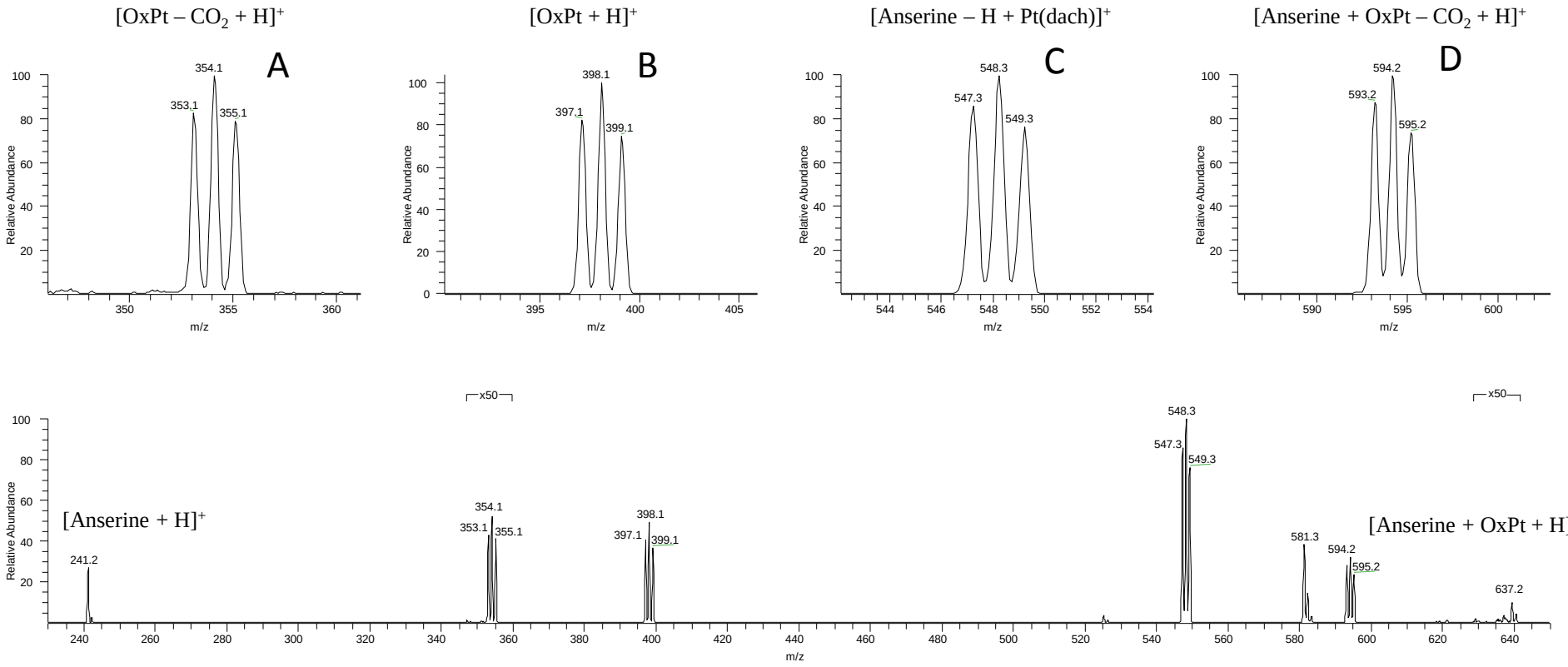

Figure 8: MS^2 spectrum of the entire isotopic envelope of the ion $[Anserine + OxPt + H]^+$ generated at 25 eV in the lab frame and isolated from the full scan spectrum of a (2:1) molar mixture of Anserine and OxPt in a (1:1) (v/v) water/methanol solution as obtained on the LTQ without allowing for incubation time. The sections of the spectrum shown under "x50" signify the magnification of the signal by 50 fold for clarity. The signals assigned as $[OxPt – CO_2 + H]^+$, $[OxPt + H]^+$, $[Anserine – H + Pt(dach)]^+$ and $[Anserine + OxPt – CO_2 + H]^+$ are each expanded and normalized to 100% in inserts A through D respectively for clarity.

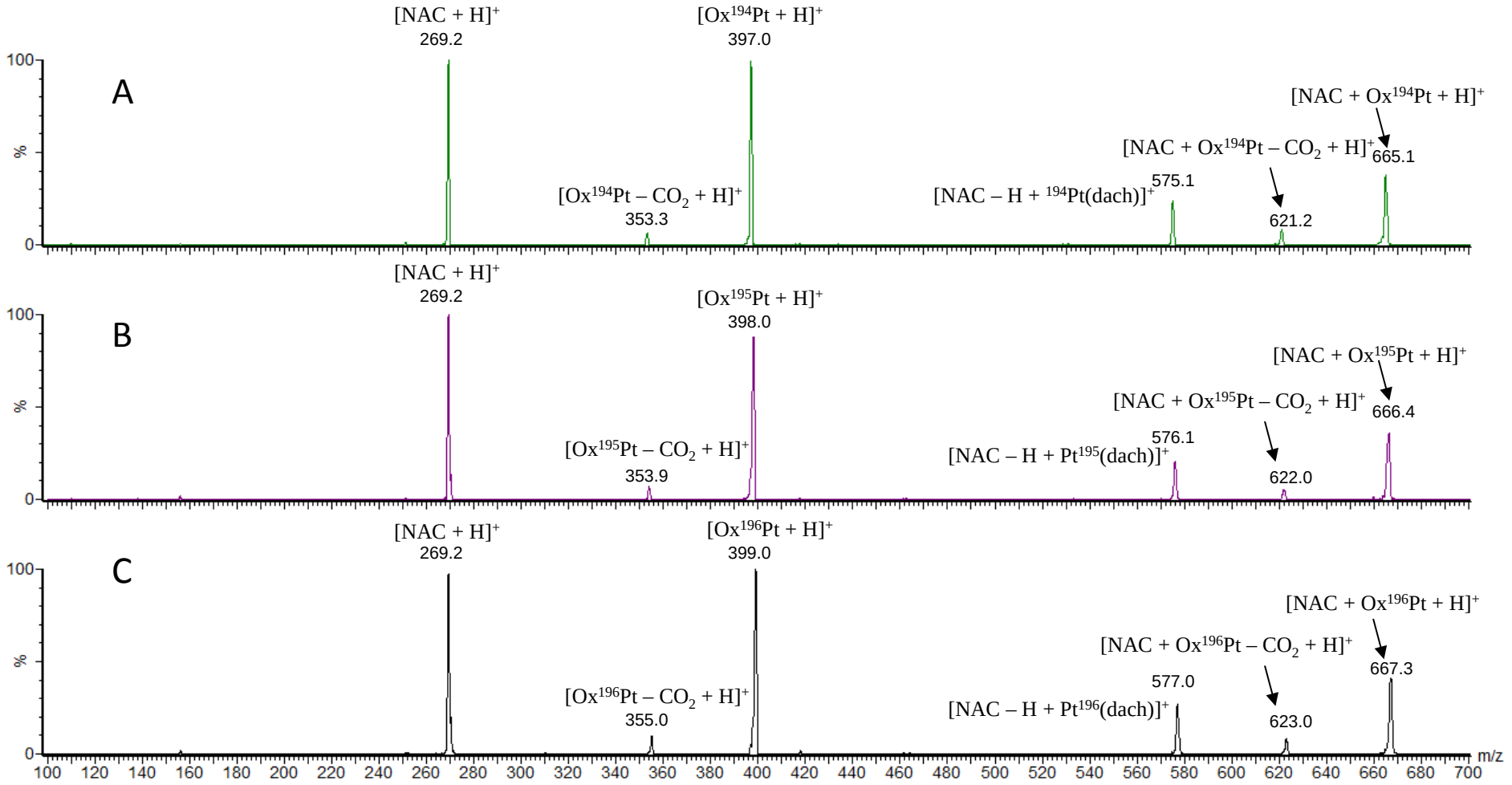

Figure 9: MS^2 spectrum of the ion [N-acetyl-carnosine + OxPt + H]$^+$ generated at 20 eV in the lab frame and isolated from the full scan spectrum of a (2:1) molar mixture of N-acetyl-carnosine (NAC in this Figure) and OxPt in a (1:1) (v/v) water/methanol solution as obtained on the Acquity TQ without allowing for incubation time. Panels A, B and C show the CID patterns obtained due to the isotopes ^{194}Pt, ^{195}Pt and ^{196}Pt of [N-acetyl-carnosine + OxPt + H]$^+$ respectively.

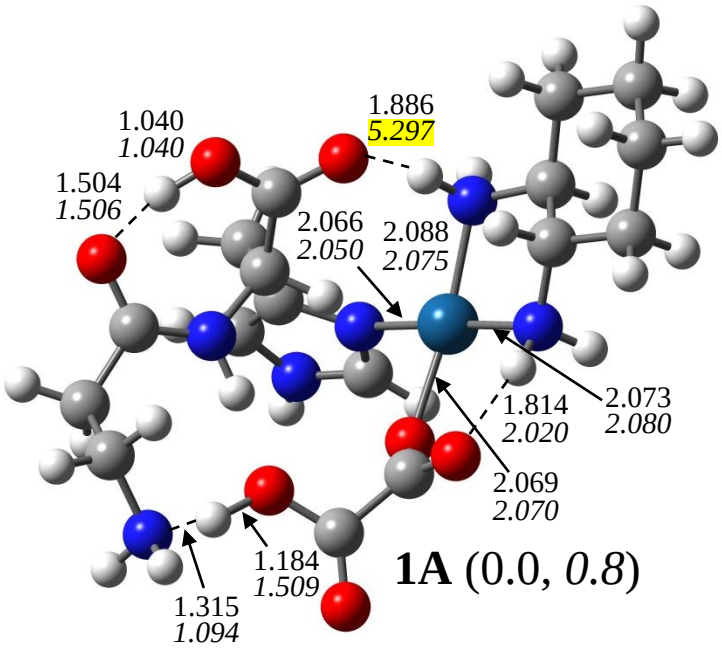

1A (0.0, *0.8*)

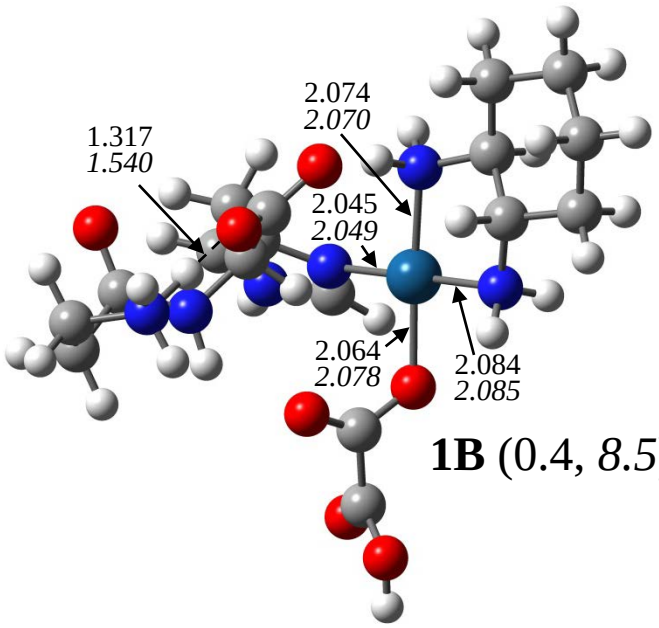

1B (0.4, *8.5*)

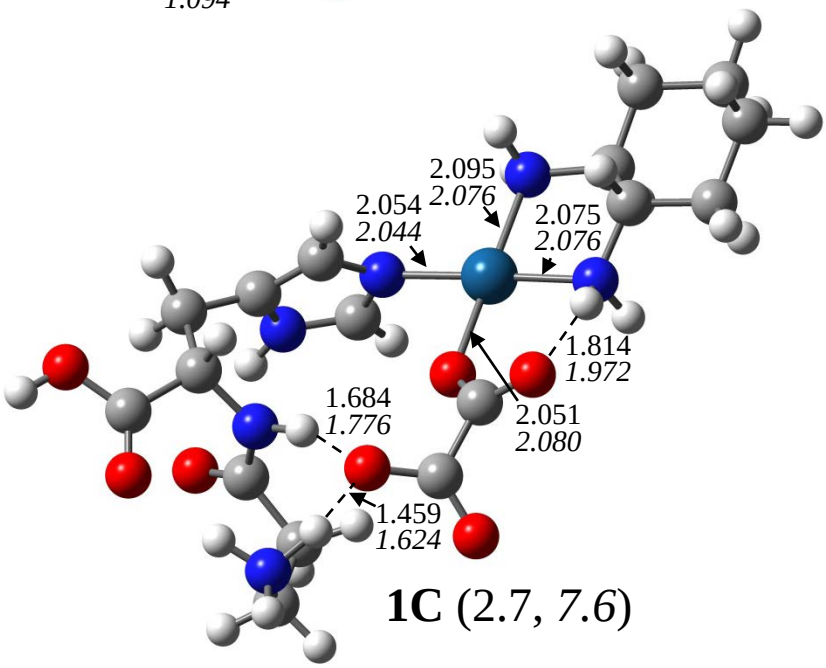

1C (2.7, *7.6*)

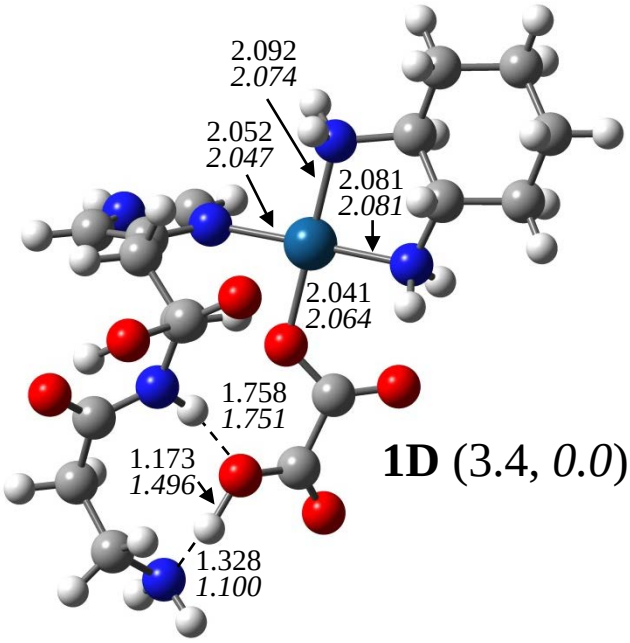

1D (3.4, *0.0*)

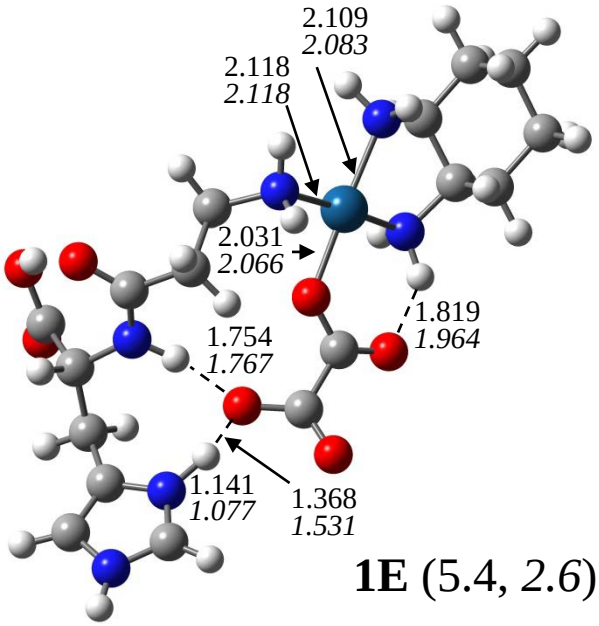

1E (5.4, *2.6*)

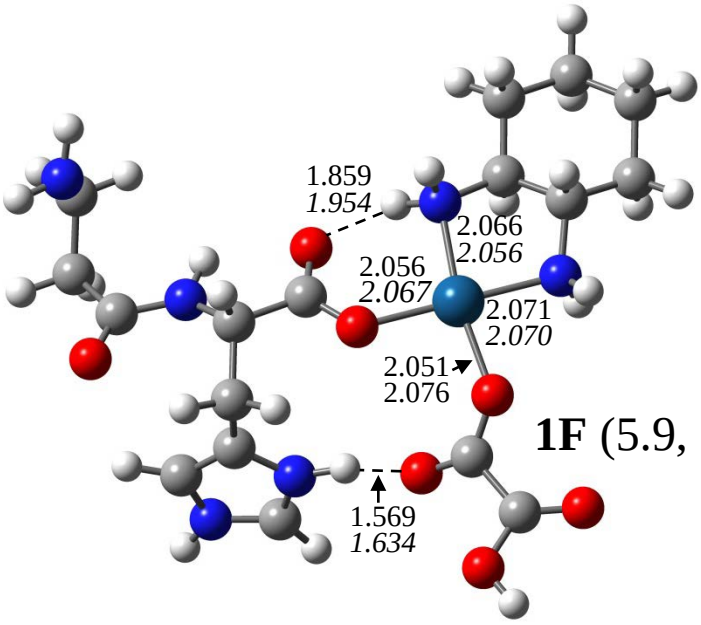

1F (5.9, *15.6*)

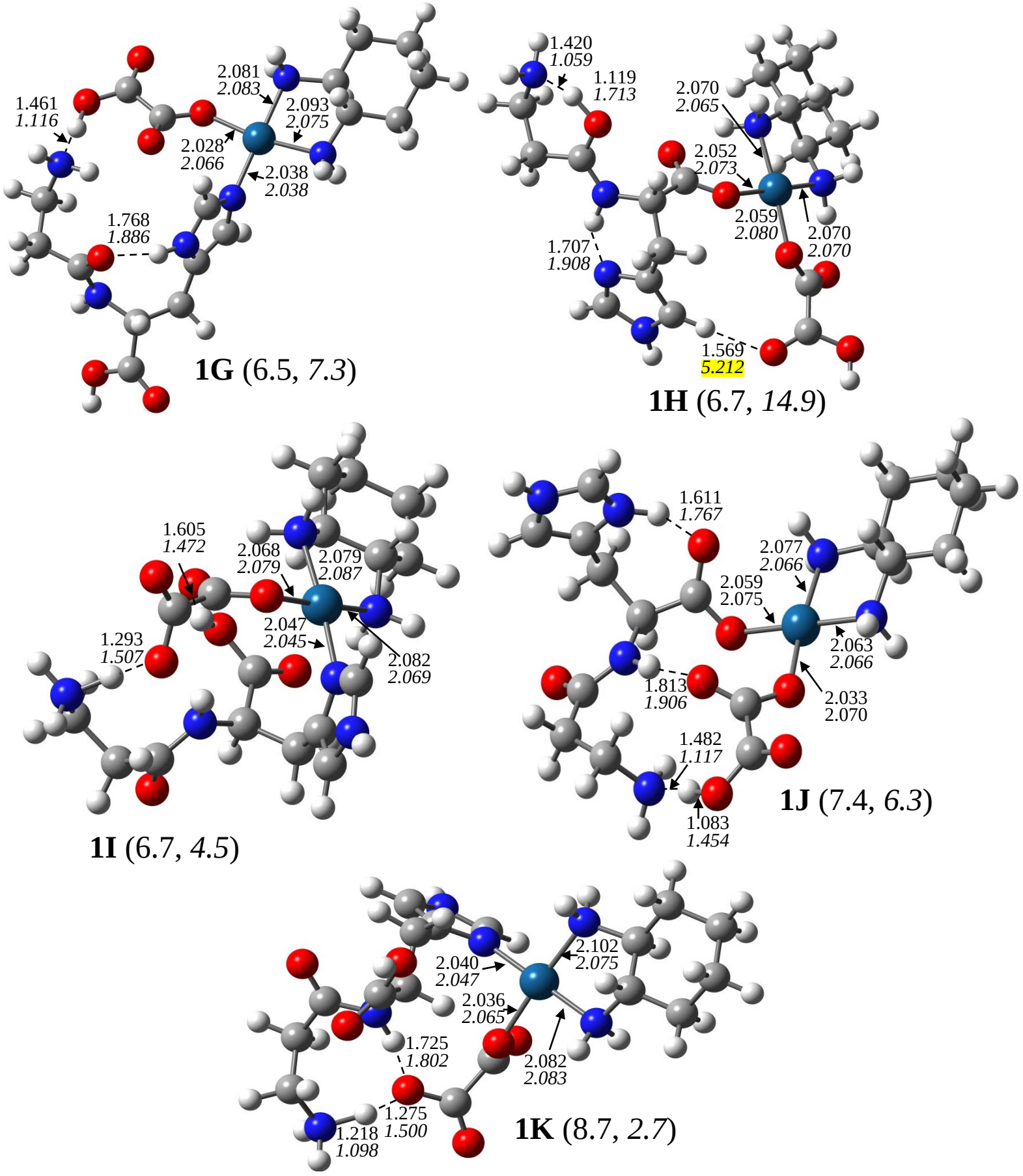

Figure 10: Structures for [Carnosine + OxPt + H]$^{+}$ ions in which a formal Pt coordination to carnosine is observed as calculated at the B3LYP/LANL2DZ level of theory. Bond lengths are in Angstroms, relative free energies are indicated in parenthesis. Italicized numbers are for solvated species.

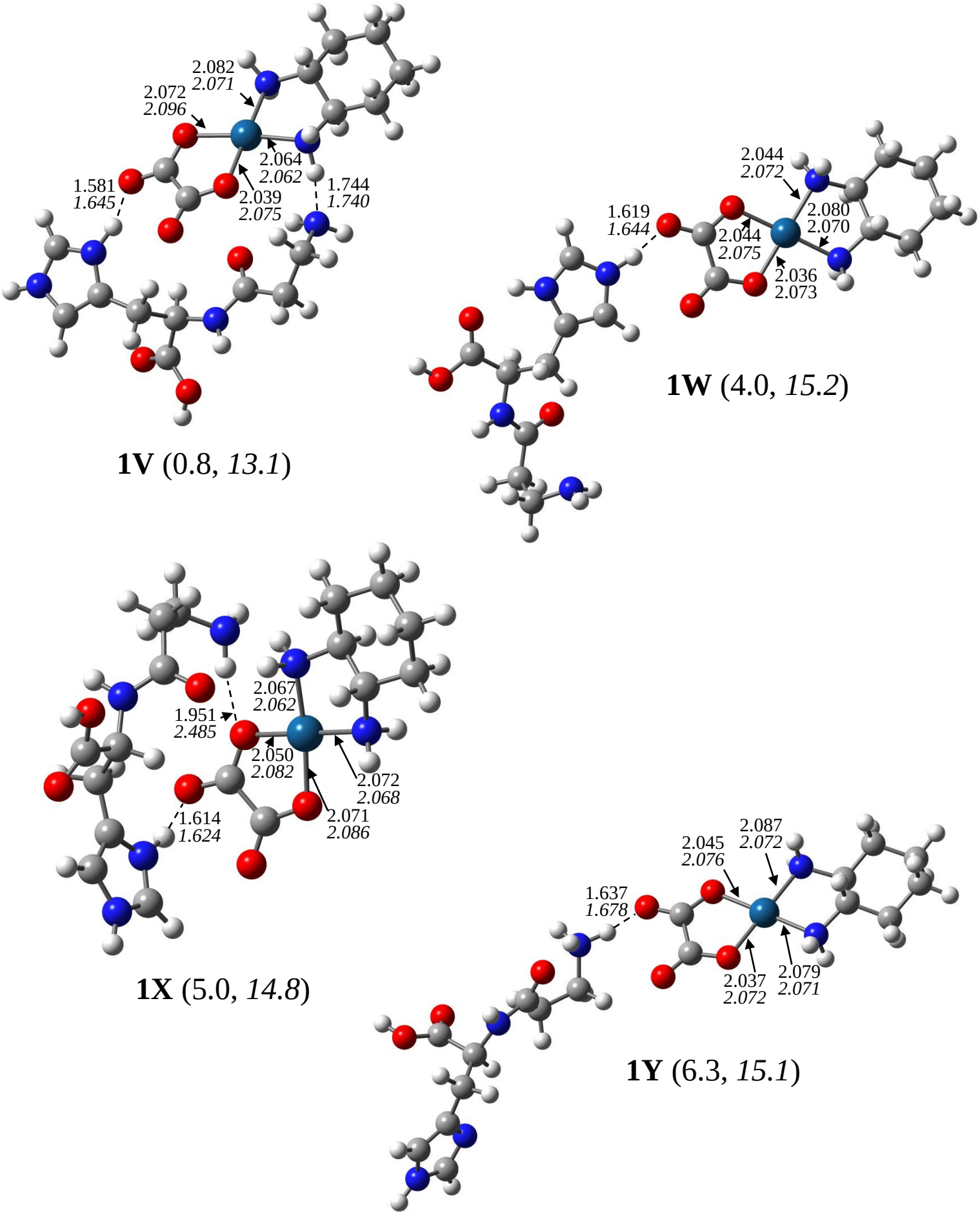

Figure 11: Structures for [Carnosine + OxPt + H]$^{+}$ ions in which no formal Pt coordination to carnosine is observed as calculated at the B3LYP/LANL2DZ level of theory. Bond lengths are in Angstroms, relative free energies are indicated in parenthesis. Italicized numbers are for solvated species.

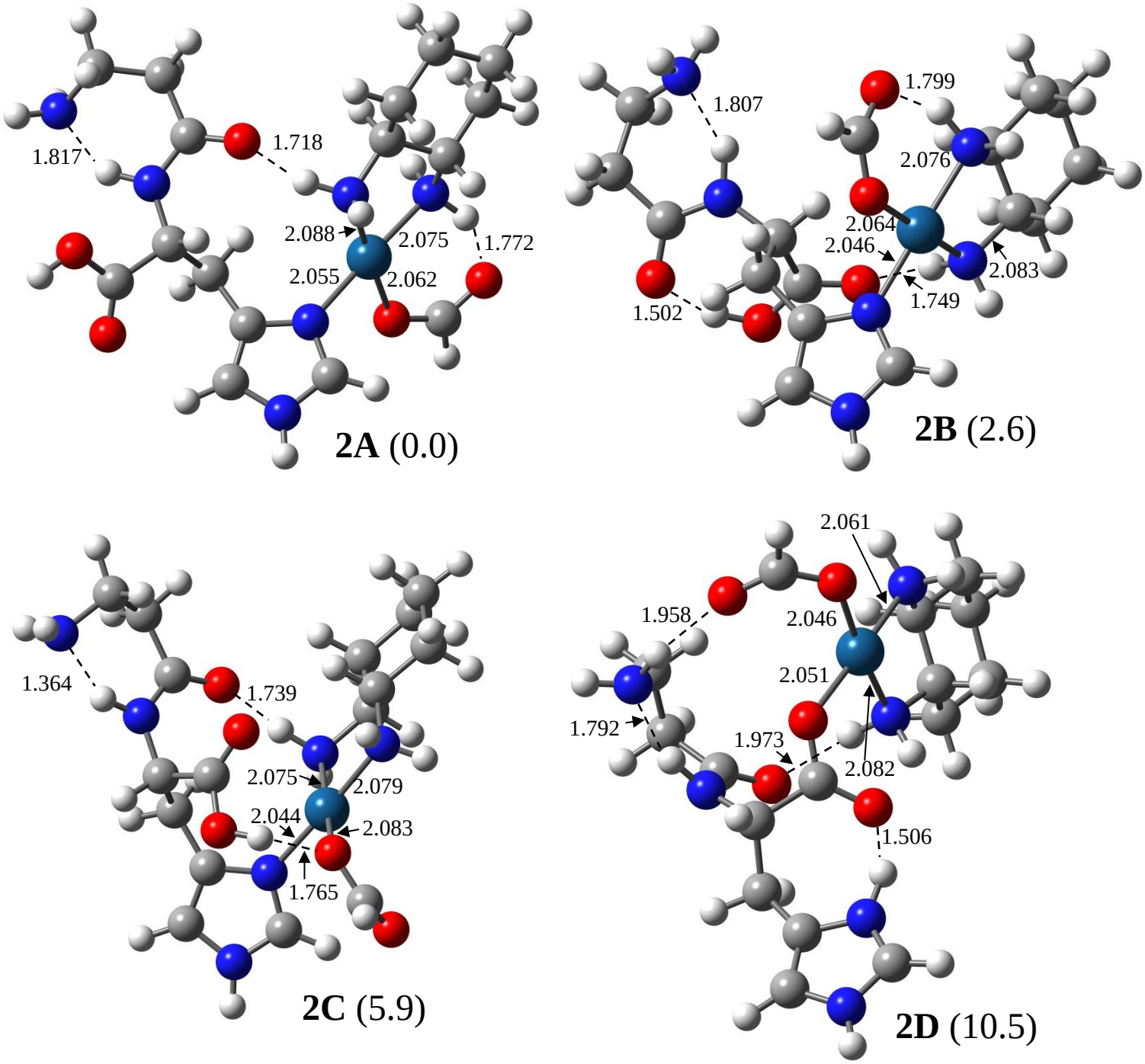

Figure 12: Structures for [Carnosine + OxPt – CO_2 + H]$^+$ ions as calculated at the B3LYP/LANL2DZ level of theory. Bond lengths are in Angstroms, relative free energies are indicated in parenthesis.

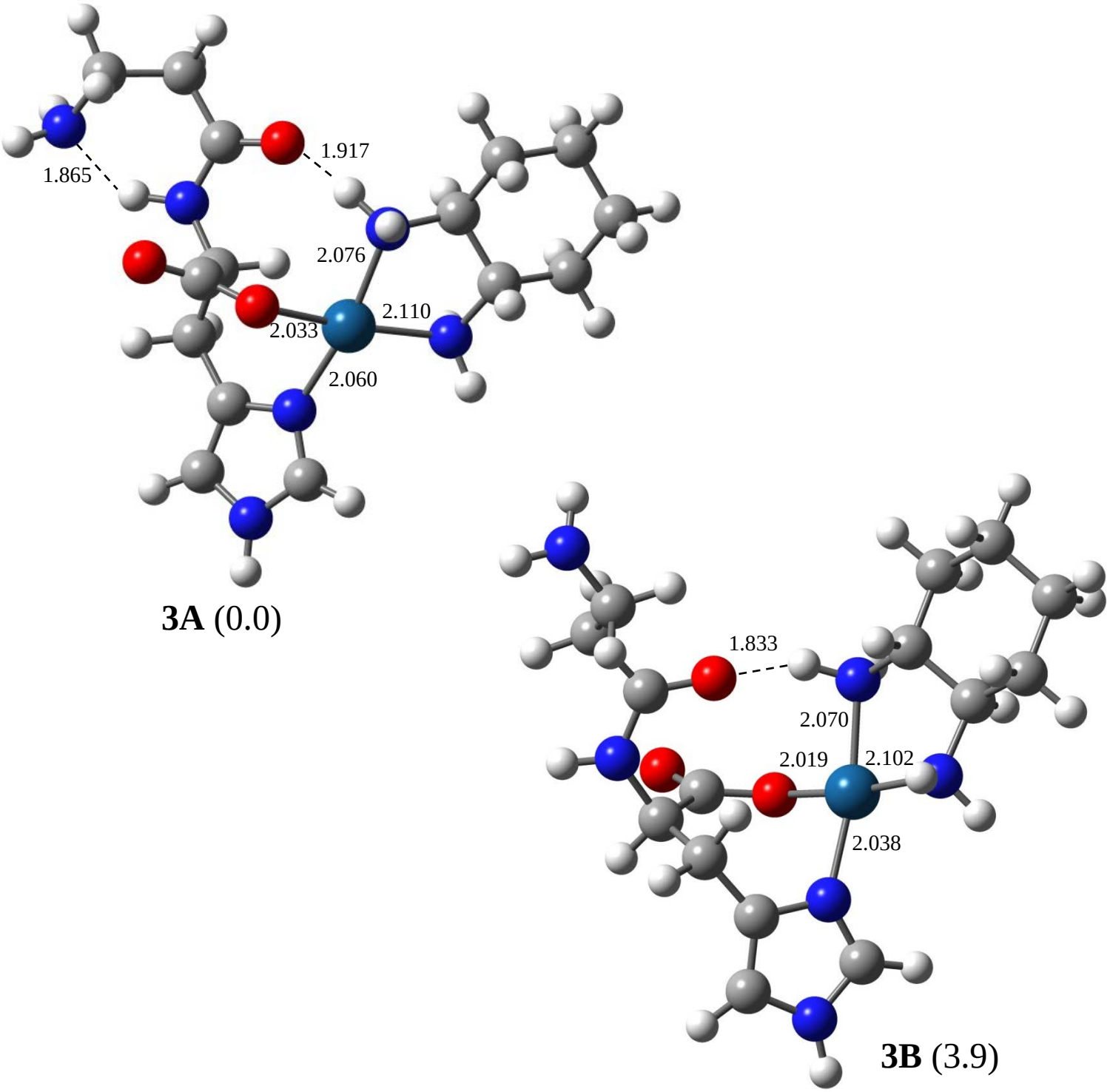

Figure 13: Structures for [Carnosine – H + Pt(dach)]$^{+}$ ions as calculated at the B3LYP/LANL2DZ level of theory. Bond lengths are in Angstroms, relative free energies are indicated in parenthesis.

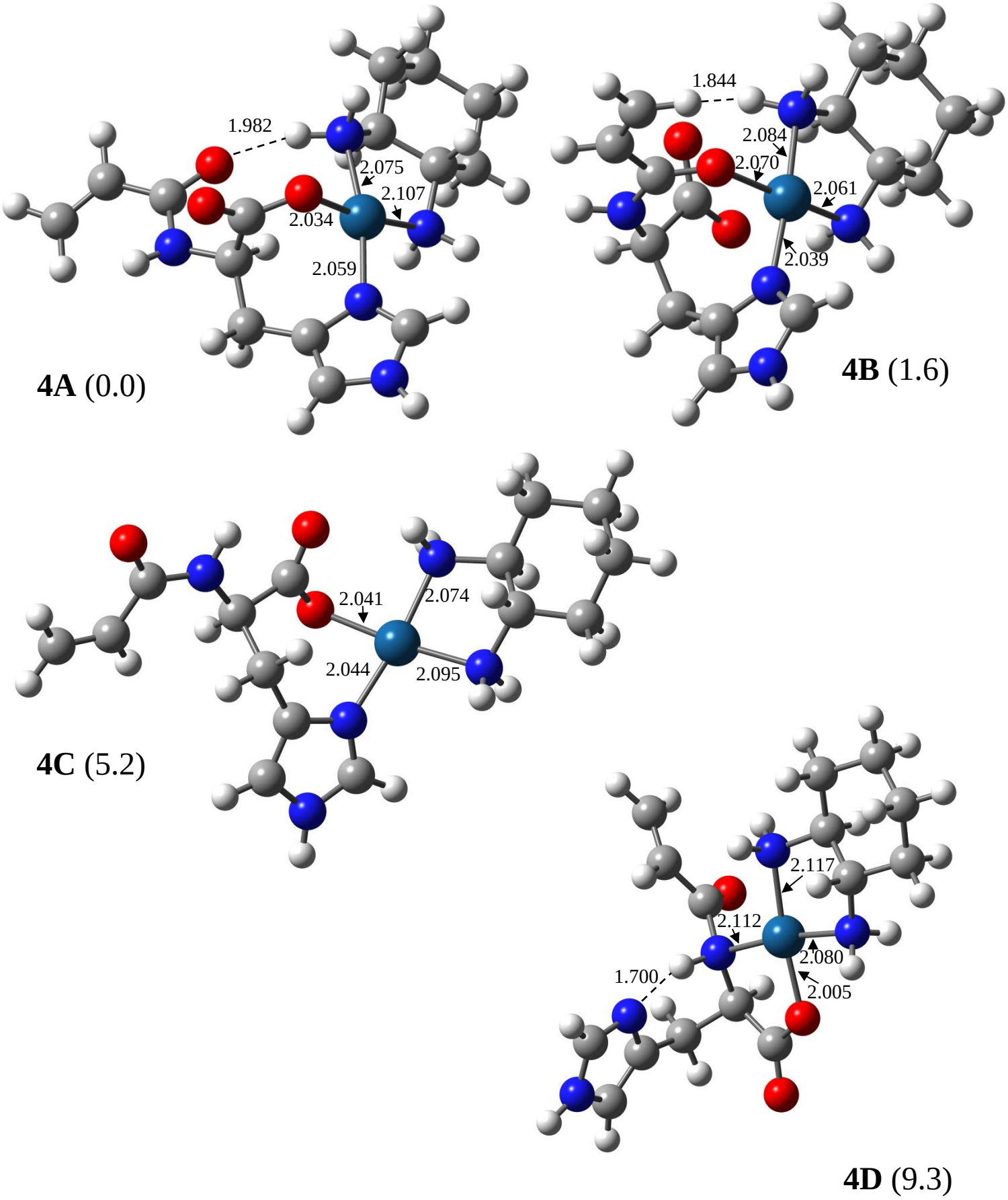

Figure 14: Structures for [Carnosine – NH_3 – H + Pt(dach)]$^+$ ions as calculated at the B3LYP/LANL2DZ level of theory. Bond lengths are in Angstroms, relative free energies are indicated in parenthesis.

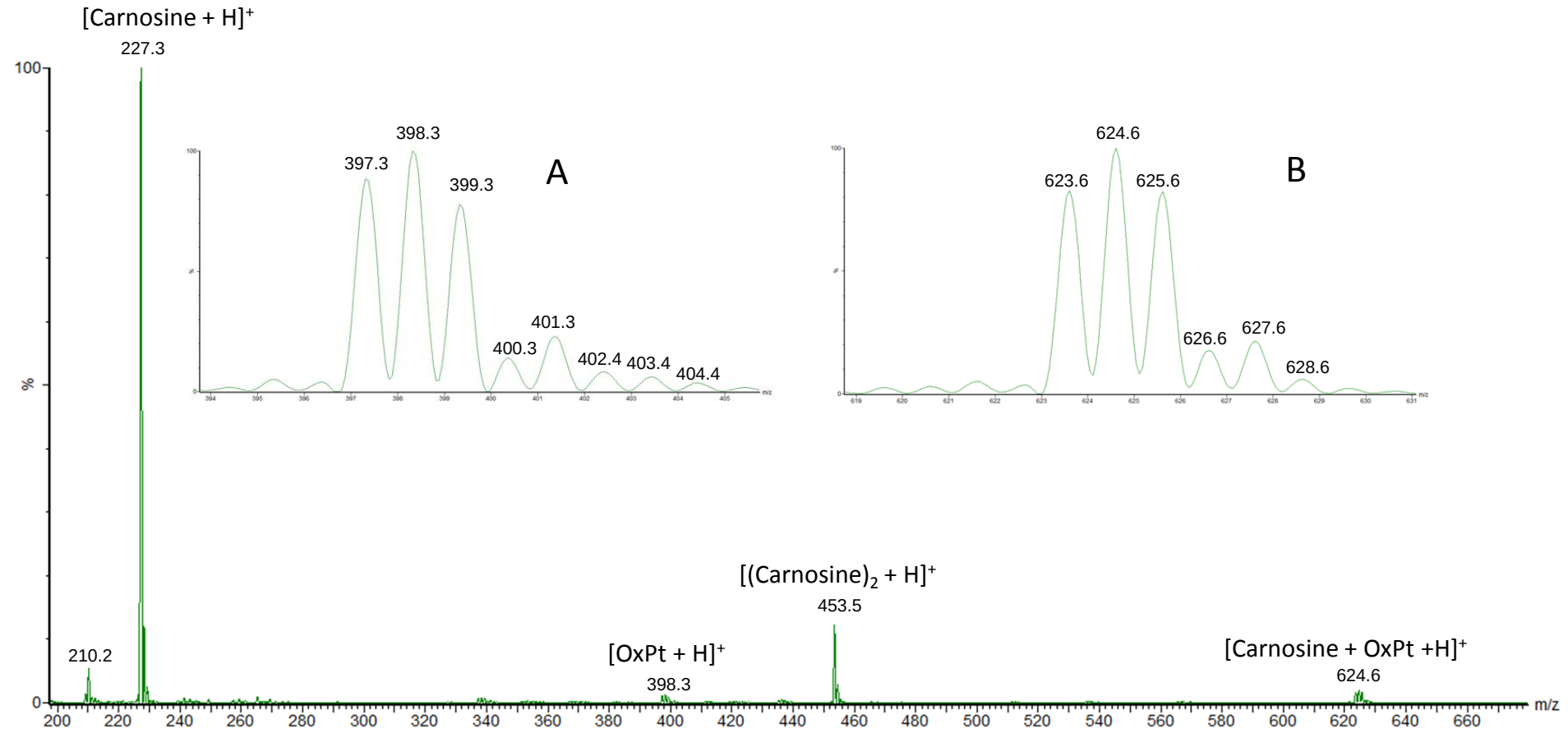

Figure S1: Full scan MS spectrum of a (2:1) molar mixture of Carnosine and OxPt in a (1:1) (v/v) water/methanol solution as obtained on the Acquity TQ without allowing for incubation time. The signals assigned as $[OxPt + H]^+$ and $[Carnosine + OxPt + H]^+$ are each expanded and normalized to 100% in inserts A and B respectively for clarity.

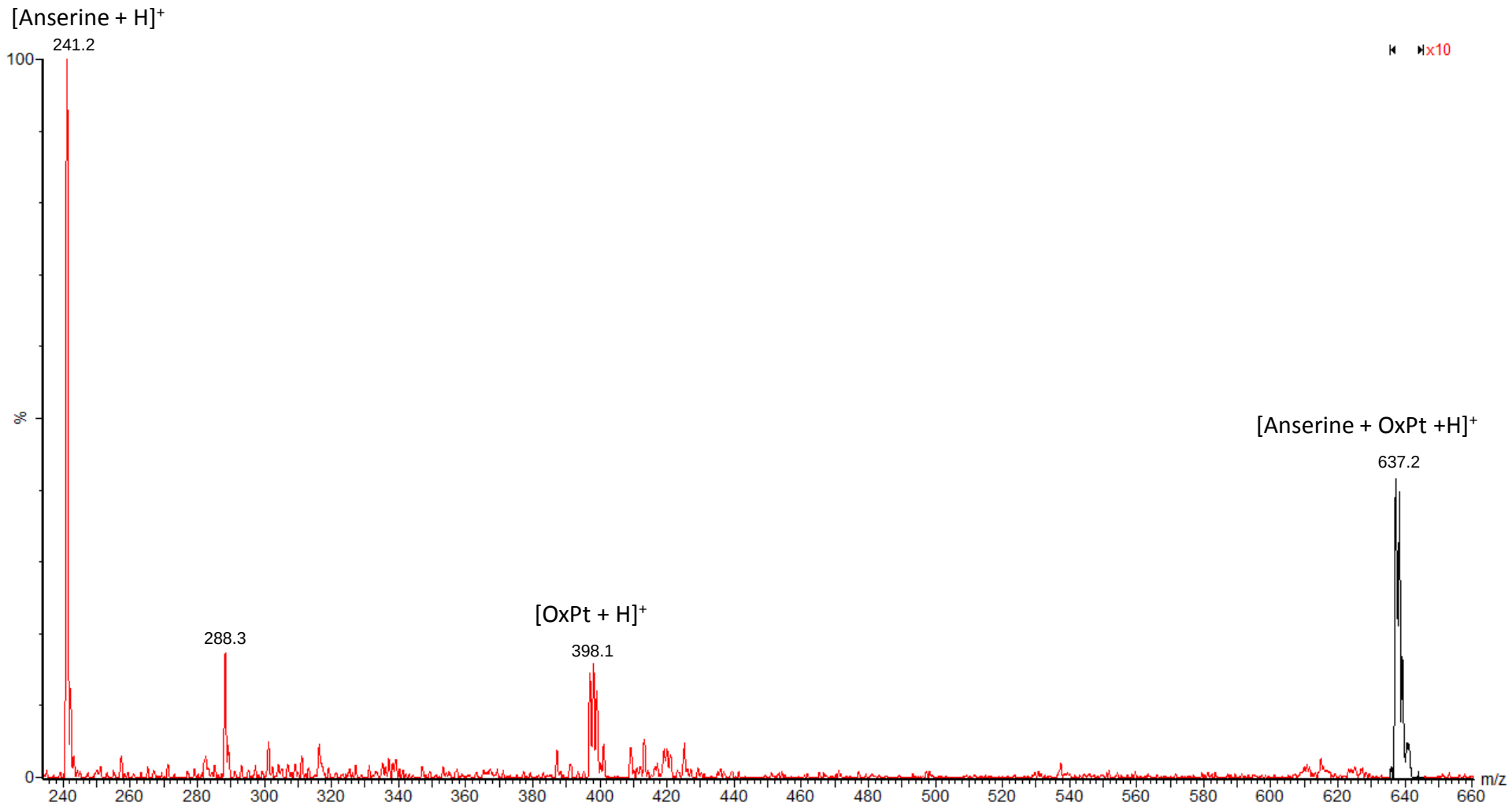

Figure S2: Full scan MS spectrum of a (2:1) molar mixture of Anserine and OxPt in a (1:1) (v/v) water/methanol solution as obtained on the XEVO TQ without allowing for incubation time. The section of the spectrum shown under "x10" signify the magnification of the signal by 10 fold for clarity. This magnification means that for example the intensity of the ion at m/z 637.2 is about 4% of the base peak.

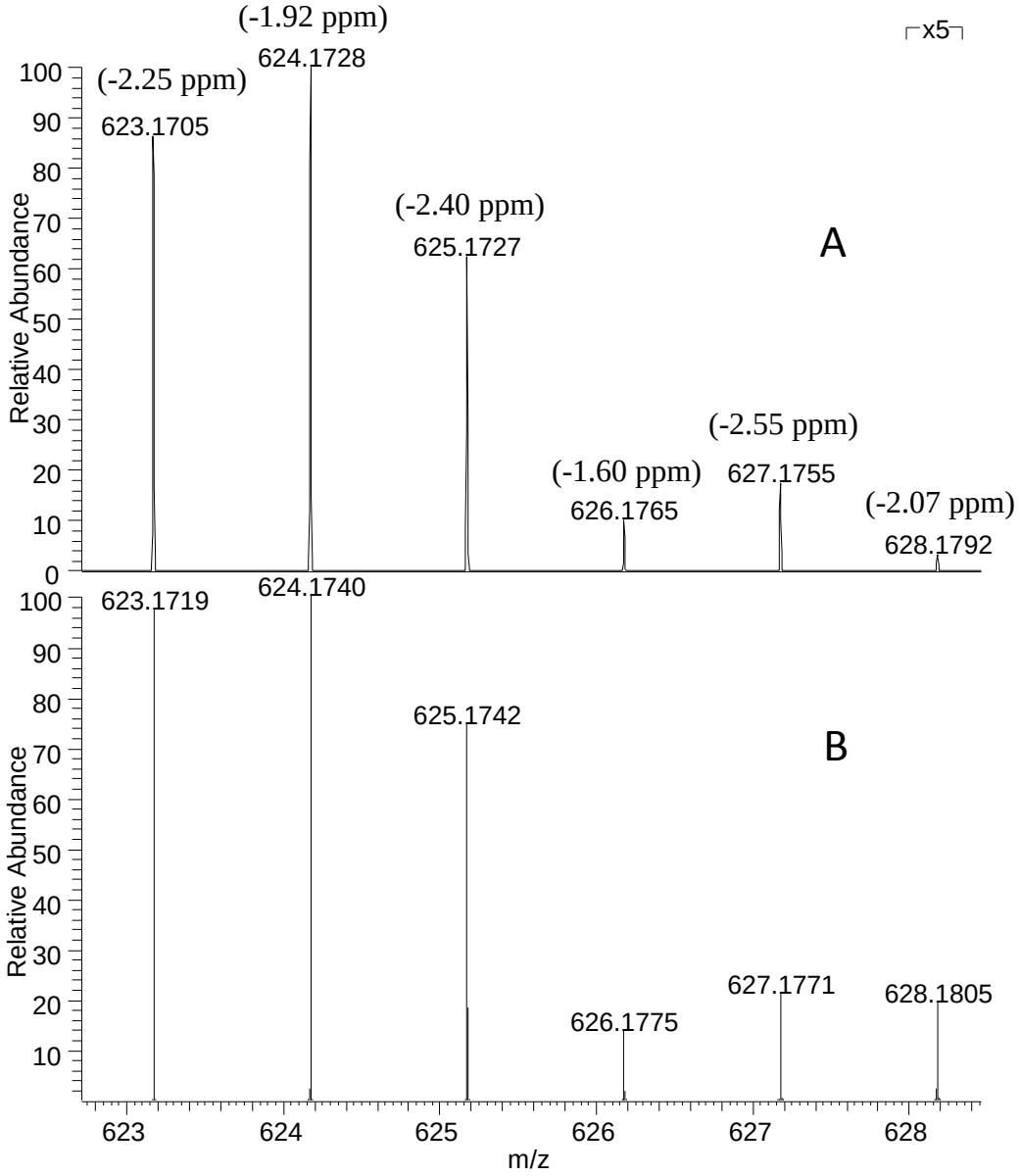

Figure S3: Full scan MS spectrum of a (2:1) molar mixture of Carnosine and OxPt in a (1:1) (v/v) water/methanol solution as obtained on the Q-Exactive FT-MS without allowing for incubation time showing the isotopic pattern of [Carnosine + OxPt +H]$^+$. The sections of the spectrum shown under "x5" signify the magnification of the signal by 5 fold for clarity. Panel A shows the experimental data wile Panel B shows the theoretically modeled spectrum using the Thermo Xcalibur software. Errors in ppm are listed next to each of the experimental isotopic peaks observed.

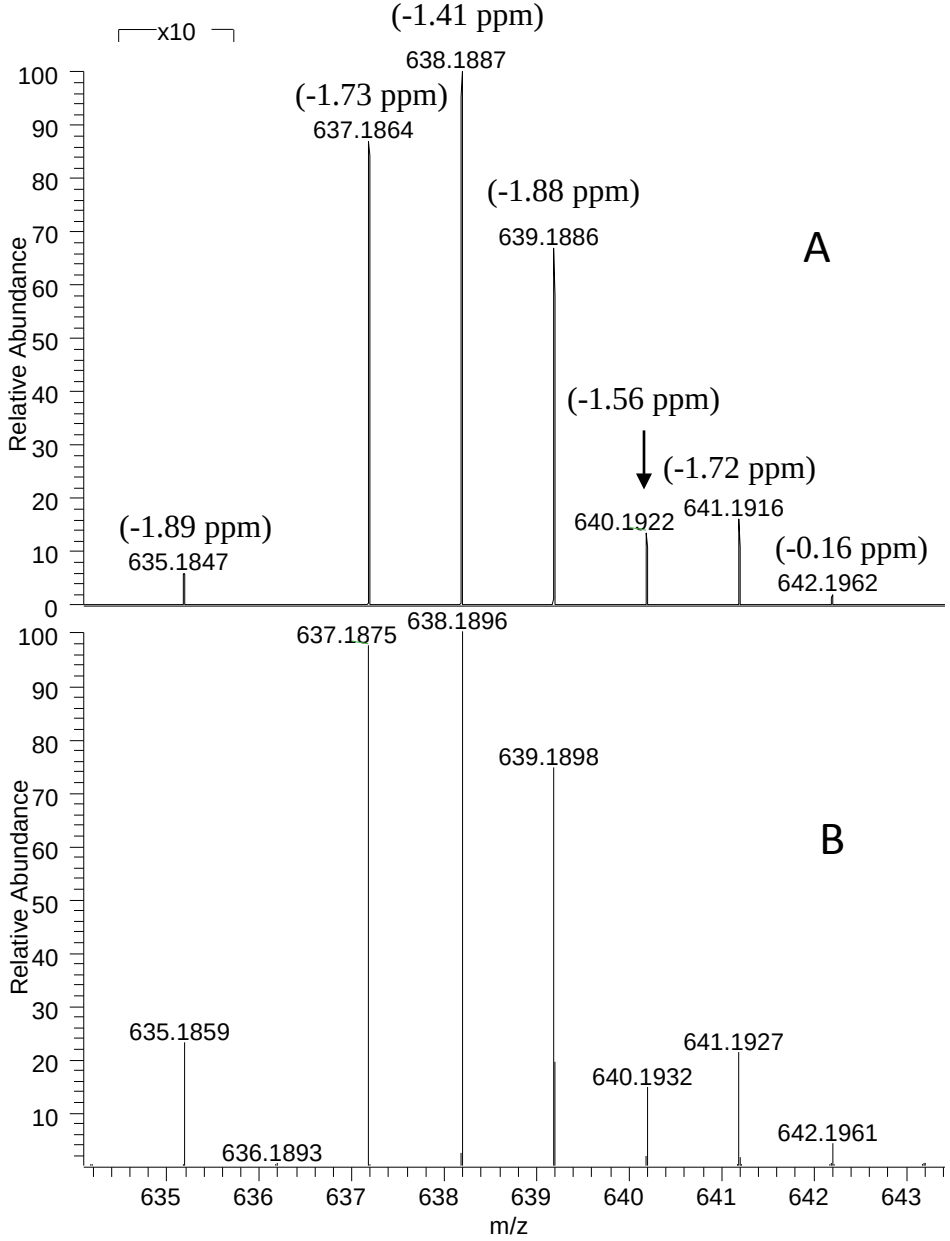

Figure S4: Full scan MS spectrum of a (2:1) molar mixture of Anserine and OxPt in a (1:1) (v/v) water/methanol solution as obtained on the Q-Exactive FT-MS without allowing for incubation time showing the isotopic pattern of [Anserine + OxPt +H]$^+$. The sections of the spectrum shown under "x10" signify the magnification of the signal by 10 fold for clarity. Panel A shows the experimental data wile Panel B shows the theoretically modeled spectrum using the Thermo Xcalibur software. Errors in ppm are listed next to each of the experimental isotopic peaks observed.

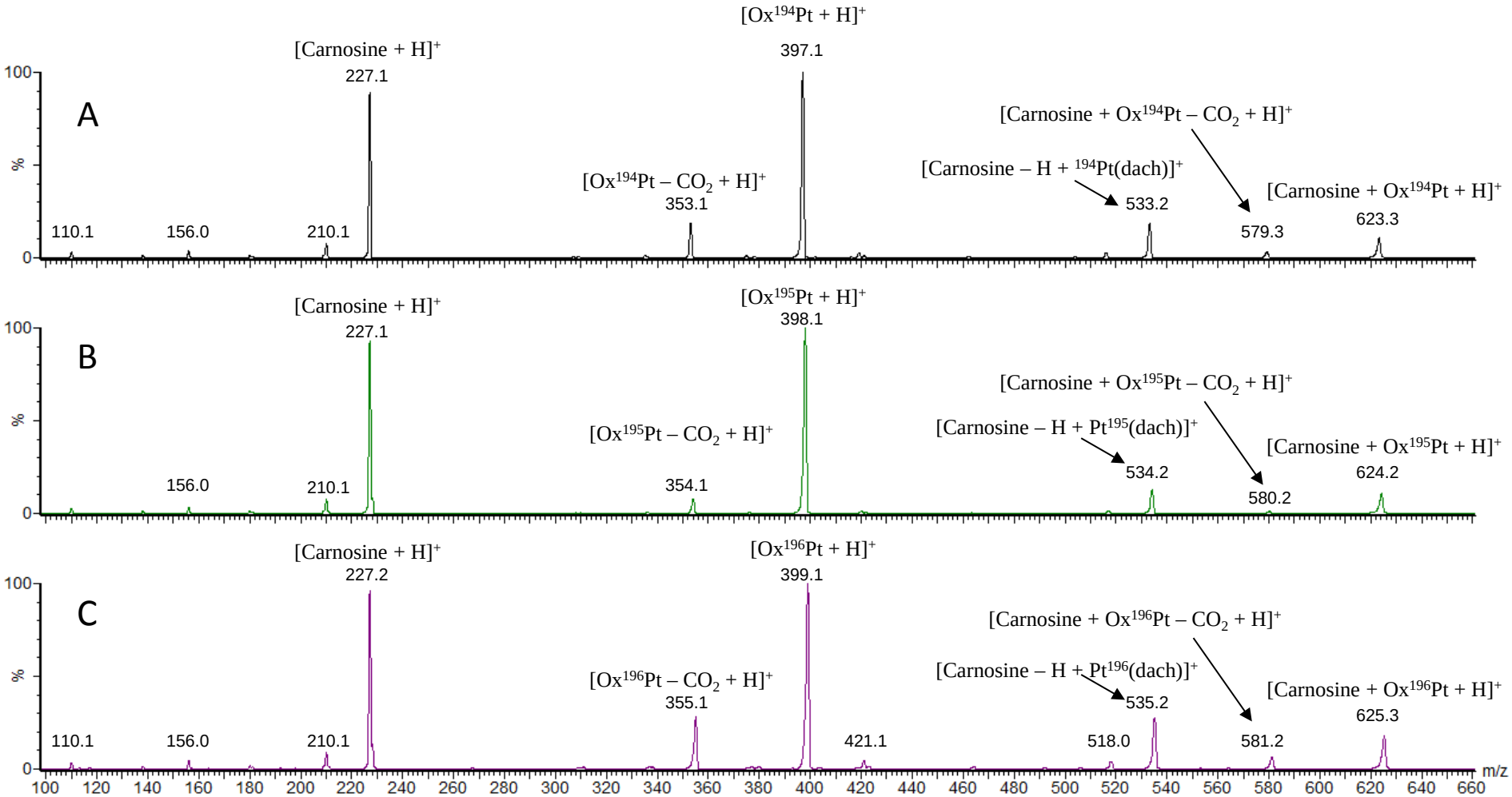

Figure S5: MS^2 spectrum of the ion [Carnosine + OxPt + H]$^+$ generated at 25 eV in the lab frame and isolated from the full scan spectrum of a (2:1) molar mixture of Carnosine and OxPt in a (1:1) (v/v) water/methanol solution as obtained on the Acquity TQ without allowing for incubation time. Panels A, B and C show the CID patterns obtained due to the isotopes ^{194}Pt, ^{195}Pt and ^{196}Pt of [Carnosine + OxPt + H]$^+$ respectively.

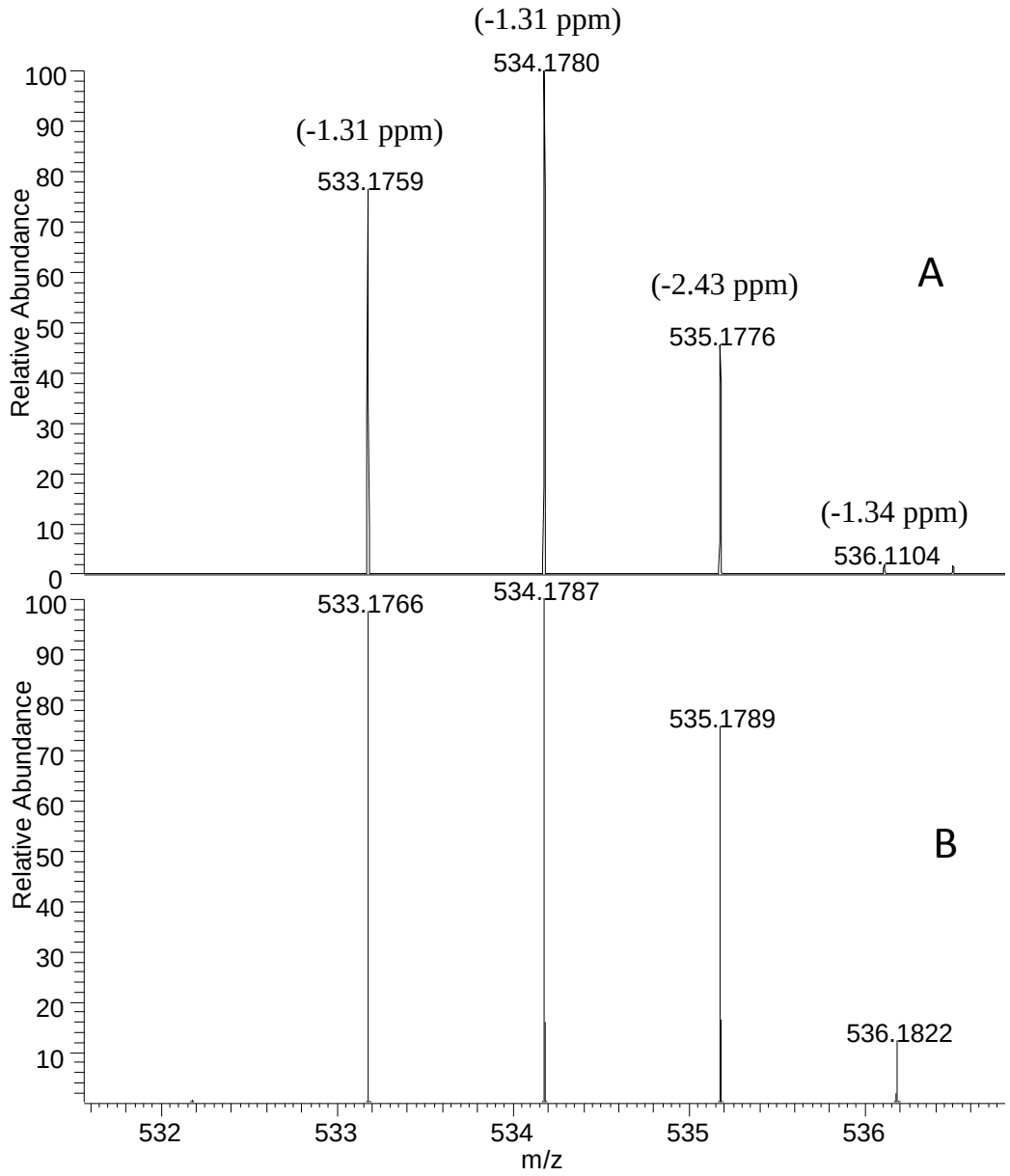

Figure S6: Tandum mass spectra of a (2:1) molar mixture of Carnosine and OxPt in a (1:1) (v/v) water/methanol solution as obtained on the Q-Exactive FT-MS without allowing for incubation time showing the isotopic pattern of [Carnosine – H + Pt(dach)]$^{+}$. Panel A shows the experimental data wile Panel B shows the theoretically modeled spectrum using the Thermo Xcalibur software. Errors in ppm are listed next to each of the experimental isotopic peaks observed. Errors in ppm are listed next to each of the experimental isotopic peaks observed.

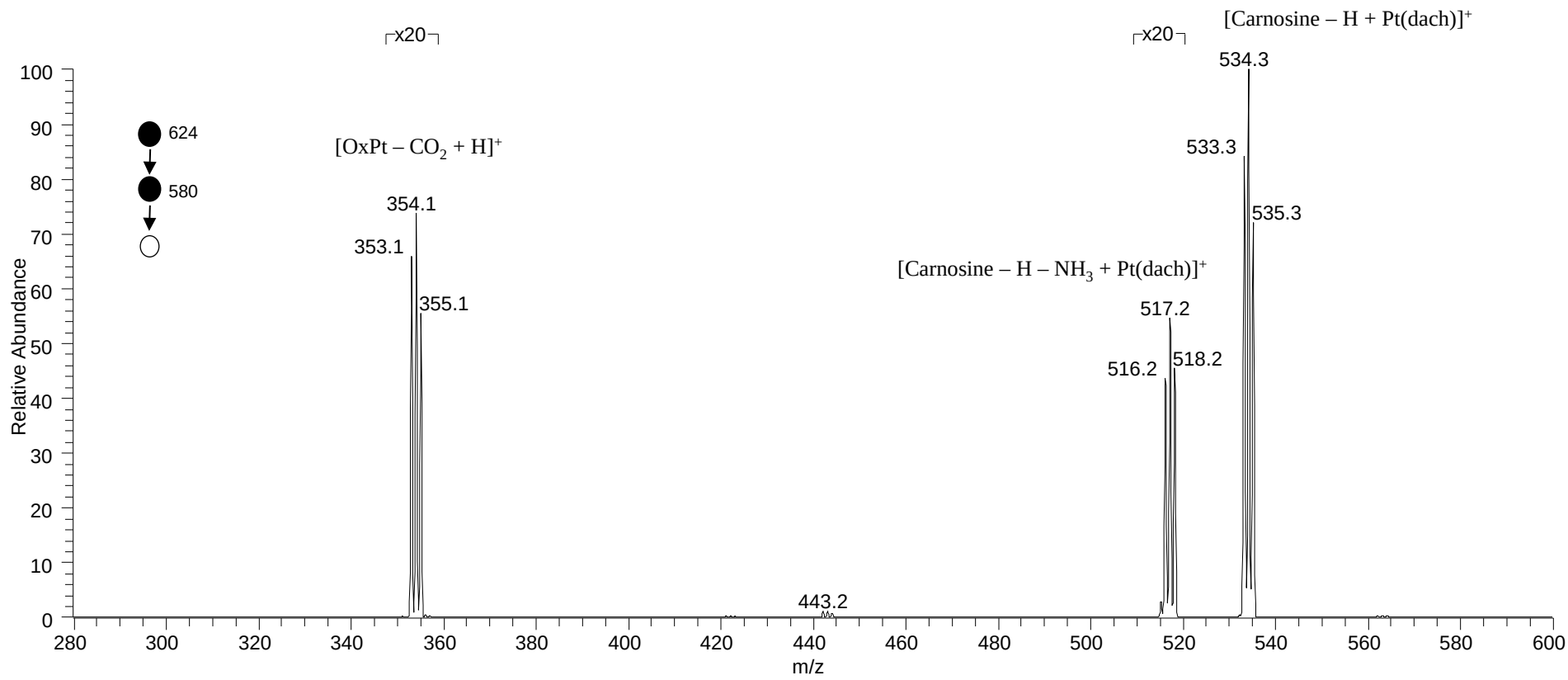

Figure S7: Tandem mass spectra of the fragment ion cluster centered around m/z 580 generated and isolated from the CID of [Carnosine + OxPt + H]$^+$ at 30 eV in the lab frame which is in turn isolated from the full scan spectrum of a (2:1) molar mixture of Carnosine and OxPt in a (1:1) (v/v) water/methanol solution as obtained on the LTQ.

Table S1: Electronic energies, Zero-Point Vibrational Energies, Thermal Energies, Entropies and relative free energies for species calculated at B3LYP\LANL2DZ. Italicized values are for PCM calculations in a water solvent. Structures **1A-1U** refer to [Carnosine + OxPt + H]$^+$ in which direct Pt bonding to carnosine is observed. Structures **1V-1Y** refer to [Carnosine + OxPt + H]$^+$ in which no direct Pt bonding to carnosine is observed. Structures **2A-2N**, **3A-3G**, **4A-4M** and **5A-5B** refer to [Carnosine + OxPt – CO_2 + H]$^+$, [Carnosine – H + Pt(dach)]$^+$, [Carnosine – NH_3 – H + Pt(dach)]$^+$ and [OxPt – CO_2 + H]$^+$ respectively.

Structure	Electronic energy (Hartrees)	ZPE (kcal mol^{-1})	$\mathbf{H^o_{298} - H^o_0}$ (kcal mol^{-1})	Entropy (cal mol^{-1} K^{-1})	Relative free energy at 298 K (kcal mol^{-1})
1A	-1639.2886242	312.6	19.6	196.8	0.0
	-1639.4050202	*314.6*	*19.9*	*201.1*	*0.8*
1B	-1639.2858222	312.8	20.0	203.4	0.4
	-1639.3913698	*314.5*	*20.1*	*204.5*	*8.5*
1C	-1639.2867573	314.4	19.6	197.5	2.7
	-1639.3956112	*315.2*	*19.8*	*200.1*	*7.6*
1D	-1639.2796868	312.7	20.0	205.4	3.4
	-1639.4041530	*314.2*	*20.0*	*204.7*	*0.0*
1E	-1639.2784107	313.5	19.8	203.6	5.4
	-1639.4015638	*314.5*	*19.7*	*201.5*	*2.6*
1F	-1639.2732867	312.9	20.7	213.8	5.9
	-1639.3731196	*312.8*	*20.8*	*215.6*	*15.6*
1G	-1639.2758092	312.9	20.1	204.4	6.5
	-1639.3914762	*314.0*	*20.3*	*207.1*	*7.3*
1H	-1639.2729851	312.2	20.1	207.4	6.7
	-1639.3770276	*314.2*	*20.5*	*213.3*	*14.9*
1I	-1639.2778140	312.9	19.7	198.0	6.7
	-1639.3970803	*313.9*	*20.1*	*203.7*	*4.5*
1J	-1639.2760210	313.7	19.8	202.3	7.4
	-1639.3961354	*314.9*	*19.9*	*202.4*	*6.3*
1K	-1639.2716859	312.5	20.2	204.9	8.7
	-1639.3958654	*314.3*	*20.3*	*214.4*	*2.7*
1L	-1639.2723656	312.9	20.3	206.1	8.3
	-1639.3651803	*312.2*	*20.3*	*207.8*	*21.9*

1M	-1639.2680874	312.9	20.4	210.2	9.9
	-1639.3712658	*312.5*	*20.5*	*212.7*	*17.0*
1N	-1639.2702447	314.2	20.1	202.5	11.8
	-1639.3699854	*314.1*	*20.3*	*206.5*	*21.1*
1O	-1639.2751572	314.9	19.4	192.0	11.9
	-1639.3845742	*313.7*	*19.7*	*197.0*	*13.7*
1P	-1639.2677622	313.4	20.2	204.1	12.2
	-1639.3703845	*313.5*	*20.4*	*205.0*	*20.8*
1Q	-1639.2640107	313.8	19.6	200.3	15.5
	-1639.3799232	*313.8*	*19.9*	*204.8*	*14.6*
1R	-1639.2631978	313.4	20.0	201.1	15.8
	-1639.3842329	*315.0*	*20.3*	*208.0*	*12.6*
1S	-1639.2554539	314.0	20.2	207.2	19.6
	-1639.3634689	*313.5*	*20.3*	*209.7*	*23.6*
1T	-1639.2554538	314.0	20.2	207.2	19.6
	-1639.3634688	*313.5*	*20.3*	*209.7*	*23.6*
1U	-1639.2500998	312.1	20.6	212.9	19.8
	-1639.3468289	*311.9*	*20.7*	*214.6*	*31.4*
1V	-1639.2855972	313.4	20.1	204.5	0.8
	-1639.3803957	*313.2*	*20.4*	*208.5*	*13.1*
1W	-1639.2750738	312.9	20.7	216.3	4.0
	-1639.3730479	*312.7*	*20.8*	*217.2*	*15.2*
1X	-1639.2806661	313.8	20.0	202.2	5.0
	-1639.3792743	*313.5*	*20.3*	*206.4*	*14.8*
1Y	-1639.2698582	313.8	20.6	219.8	7.1
	-1639.3745151	*314.0*	*20.7*	*218.0*	*15.1*
2A	-1450.7542132	304.6	18.5	192.5	0.0
2B	-1450.7521575	304.7	18.1	187.2	2.6
2C	-1450.7488908	305.0	18.2	184.3	5.9
2D	-1450.7396653	304.6	18.2	186.7	10.5
2E	-1450.7359210	304.2	18.4	189.4	11.9
2F	-1450.7356931	304.0	18.2	186.5	12.5

2G	-1450.7278354	303.5	18.6	198.1	13.9
2H	-1450.7225517	305.3	18.3	190.2	21.0
2I	-1450.7156471	305.4	18.5	193.8	24.6
2J	-1450.6987011	302.4	18.6	191.6	33.0
2K	-1450.6951026	303.3	18.8	199.0	34.1
2L	-1450.6961826	302.4	18.3	188.4	35.3
2M	-1450.6910914	302.8	18.4	189.3	38.6
2N	-1450.6692231	302.7	19.0	199.4	49.9
3A	-1260.9744123	282.5	15.8	168.1	0.0
3B	-1260.9646407	281.5	16.4	174.2	3.9
3C	-1260.9499510	283.0	15.7	171.6	14.8
3D	-1260.9471698	282.5	15.6	164.1	18.1
3E	-1260.9382042	283.1	15.3	159.5	25.4
3F	-1260.8792520	280.7	16.1	171.0	57.3
3G	-1260.8353995	281.2	15.5	163.5	86.9
4A	-1204.3891678	256.0	15.1	162.6	0.0
4B	-1204.3888797	256.2	14.7	157.3	1.6
4C	-1204.3795752	255.7	15.1	164.3	5.2
4D	-1204.3716679	255.2	15.1	166.1	9.3
4E	-1204.3753032	256.7	14.6	159.2	10.0
4F	-1204.3612046	255.2	14.9	161.7	16.8
4G	-1204.3318604	255.0	14.9	162.3	34.9
4H	-1204.3247413	254.8	15.1	166.2	38.2
4I	-1204.3241914	255.0	15.0	163.8	39.4
4J	-1204.3113922	254.7	14.8	158.9	48.4
4K	-1204.2953955	255.0	14.7	158.5	58.8
4L	-1204.2460587	253.0	15.6	169.7	85.3
4M	-1204.2346476	252.8	15.7	166.6	93.2
5A	-654.6722639	148.4	8.1	109.6	0.0
5B	-654.6344513	145.8	9.0	121.9	18.4